Inactivation of TGFβ receptors in stem cells drives cutaneous squamous cell carcinoma

Patrizia Cammareri[1,13], Aidan M Rose[2,13], David F Vincent[1,13], Jun Wang[3], Ai Nagano[3], Silvana Libertini[1], Rachel A Ridgway[1], Dimitris Athineos[1], Philip J Coates[4], Angela McHugh[2], Celine Pourreyron[2], Jasbani H S Dayal[2], Jonas Larsson[5], Simone Weidlich[6], Lindsay C Spender[2], Gopal P Sapkota[6], Karin J Purdie[7], Charlotte M Proby[2], Catherine A Harwood[7], Irene M Leigh[2,7], Hans Clevers[8], Nick Barker[9], Stefan Karlsson[5], Catrin Pritchard[10], Richard Marais[11], Claude Chelala[3], Andrew P South[2,12], Owen J Sansom[1]* and Gareth J Inman[2]*.

[1] Cancer Research UK Beatson Institute, Institute of Cancer Sciences, Glasgow University, Glasgow, G61 1BD, UK

[2]Division of Cancer Research, School of Medicine, University of Dundee, Dundee, DD1 9SY, UK

[3]Centre for Molecular Oncology, Barts Cancer Institute, Queen Mary University of London, London, E1 4NS, UK

[4]Tayside Tissue Bank, School of Medicine, University of Dundee, Dundee, DD1 9SY, UK

[5]Molecular Medicine and Gene Therapy, Lund Strategic Center for Stem Cell Biology, Lund University, Lund, 221 00, Sweden

[6]MRC Protein Phosphorylation Unit, School of Life Sciences, University of Dundee, Dundee, DD1 5EH, UK

[7]Centre for Cutaneous Research, Barts and the London School of Medicine and Dentistry, Queen Mary University of London, E1 2AT, London, UK

[8]Hubrecht Institute, Utrecht, 3584 CT, The Netherlands

[9]Institute of Medical Biology, Immunos, 138648, Singapore

[10]Department of Biochemistry, University of Leicester, Leicester, LE1 9HN, UK

[11]The Paterson Institute for Cancer Research, Manchester, M20 4BX, UK

[12]Department of Dermatology and Cutaneous Biology, Thomas Jefferson University, Philadelphia, PA 19107, USA.

[13]These authors contributed equally to this work.

*Correspondence: Gareth J Inman, Jacqui Wood Cancer Centre, Ninewells Hospital and Medical School, Dundee, DD1 9SY. g.j.inman@dundee.ac.uk; Owen J Sansom, Cancer Research UK Beatson Institute, Garscube Estate, Glasgow, G61 1BD. o.sansom@beatson.gla.ac.uk

Abstract

Melanoma patients treated with oncogenic BRAF inhibitors can develop cutaneous squamous cell carcinoma (cSCC) within weeks of treatment, driven by paradoxical RAS/RAF/MAPK pathway activation. Here, we identify frequent *TGFBR1* and *TGFBR2* mutations in human vemurafenib-induced skin lesions and in sporadic cSCC. Functional analysis reveals these mutations ablate canonical TGFβ Smad signaling which is localised to bulge stem cells in both normal human and murine skin. MAPK pathway hyperactivation (through $Braf^{V600E}$ or $Kras^{G12D}$ knockin) and TGFβ signaling ablation (through *Tgfbr1 deletion)* in $LGR5^{+ve}$ stem cells enables rapid cSCC development in the mouse. Mutation of *Tp53* (which is commonly mutated in sporadic cSCC) coupled with *Tgfbr1* deletion in $LGR5^{+ve}$ cells also results in cSCC development. These findings indicate that $LGR5^{+ve}$ stem cells can act as cells of origin for cSCC and that RAS/RAF/MAPK pathway hyperactivation or *Tp53* mutation, coupled with loss of TGFβ signaling, are driving events of skin tumorigenesis.

Introduction

The development of epithelial tumors is generally accepted to take place over several years, involving the accumulation of mutations which drive tumor progression[1]. However, some tumors contain a relatively low mutation burden[2] and develop rapidly, without progression from benign intermediary stages, suggesting a potential stem cell origin[3]. Data from murine model systems illustrate a tumor's ability to form from both stem and differentiated cells.

Within intestinal epithelium, loss of *Apc* in the LGR5^{+ve} stem cell compartment leads to adenoma, whilst tumors rarely form from differentiated cells[4]. Conversely, we have shown that targeting *Kras*, in addition to *Apc*, can de-differentiate intestinal villi and permit tumor formation[5]. Thus, the tumor cell of origin remains unclear, as does the standard model of progression from benign tumor to malignant carcinoma.

Discord with the progression model is exemplified in the skin, which carries a high mutation burden[6]. Asymptomatic normal skin carries frequent mutations in *TP53*[7,8] and *NOTCH*[6,8]. Classic chemical carcinogenesis DMBA/TPA experiments demonstrate *Hras* mutations can lie dormant in the skin (without the addition of TPA), at no obvious consequence to the tissue[9]. Indeed even when *Ras* mutation is targeted to stem cell compartments (e.g LRIG1^{+ve} cells or bulge stem cells[10,11]), this does not lead to cancer unless there is a disruption of tissue homeostasis through wounding. These findings support the hypothesis that homeostasis within stem cell compartments plays an important tumor suppressive role in highly organised structures such as skin.

We reasoned that, in the absence of wounding, mutations in other oncogenic/tumour suppressor genes might facilitate rapid skin tumorigenesis. Using targeted sequence analysis and whole exome sequencing (WES), we identify frequent mutation in both TGFβ type 1 receptor (*TGFBR1)* and TGFβ type 2 receptor (*TGFBR2)* genes in human primary cSCC samples. IntOgen mutation analysis reveals TGFβ signaling as a pathway significantly altered by mutation and functional analysis of several TGFβ receptor mutants indicates that many of these mutations result in loss of function. Pathway activation studies reveal highly localised TGFβ signaling in both normal human and mouse hair follicle bulge stem cells. In murine skin, targeted activation of the RAS/RAF/MAPK pathway, coupled with deletion of

Tgfbr1 in LGR5^{+ve} stem cells promotes rapid development of cSCC which, in the absence of wounding, may mimic the kinetics of tumor induction in vemurafenib-induced cSCC. Combined *Tp53* mutation/inactivation coupled with *Tgfbr1* loss in LGR5^{+ve} stem cells also results in cSCC with longer latency providing a model for cSCC development without RAS activation.

RESULTS

TGFBR1 and *TGFBR2* are frequently mutated in human cSCC

Cutaneous squamo-proliferative lesions (including keratoacanthomas and cSCC) arise in a significant proportion of patients treated with the type I RAF inhibitor vemurafenib. Such lesions develop within a few weeks of treatment[12,13]. Targeted sequencing has revealed that these lesions contain a high frequency of activating mutations in *HRAS*[6,12,13]. Cutaneous lesions isolated from patients treated with sorafenib (the "pan-RAF" inhibitor) also harbour mutations in *HRAS*, *TP53* and *TGFBR1*[14]. Employing targeted deep sequencing of 39 squamo-proliferative lesions from 7 patients (including cSCC and actinic keratosis (AK); **Supplementary Table 1**) treated with vemurafenib (using a percentage variance criterion of >10%) we identified frequent coding mutations in both *TGFBR1* (8/39, 21% of samples) and *TGFBR2* (5/39, 13% of samples) revealing mutation of TGFβ receptors in 28% of lesions (**Fig. 1a, Supplementary Data 1**). These mutational events were only surpassed in frequency by mutations in *NOTCH1*/*NOTCH2* (56%) and activating mutations of *HRAS* (38%). *TP53* mutations arose in 26% of lesions[6] (**Fig. 1a, Supplementary Data 2**). In contrast to *NOTCH*, (using our mutational call cut off, see Methods) we did not detect any mutations in TGFβ receptors or *HRAS* in the normal or perilesional skin samples (n=6 from 4 patients, 3 of which had lesions containing TGFβ receptor mutations). These findings imply that a

combination of potential mutational inactivation of TGFβ signaling and activation of *HRAS* may be important driving events in vemurafenib-induced skin lesions and skin tumorigenesis.

We next sought to investigate whether loss of TGFβ signaling is a frequent event in sporadic cSCC. We employed targeted 454 pyrosequencing of *TGFBR1* and *TGFBR2* in 91 human primary cSCC samples (**Supplementary Table 2**) and 21 human cell lines derived from primary cSCC[15], all of which were recently sequenced for common genetic alterations[6]. Using a percentage variance criterion of >10% we detected mutations of *TGFBR1* in 22% and *TGFBR2* in 30% of primary cSCC samples and 14% of cell lines (**Fig. 1b**,**c** and **Supplementary Data 3**). Overall, mutation of TGFβ receptors occurred in 43% of primary cSCC samples. These mutational events were only surpassed in frequency by mutations in *NOTCH1/2* (86%), and this time *TP53* (63%) (**Fig. 1b, Supplementary Data 4, Ref 6**). In sporadic cSCC oncogenic activation of RAS only occurred in 9% of samples (**Fig. 1b, Supplementary Data 4, Ref 6**). We then sequenced normal blood samples from 8 patients with sporadic cSCC whose lesions harboured mutations in TGFβ receptors (**Supplementary Data 3**) and found no TGFβ receptor mutations. Next we prospectively collected a further Dundee cohort of 7 primary cSCC samples with complementary matched normal distant and perilesional skin (**Supplementary Table 3**). This cohort demonstrated a comparable spectrum of mutation in our selected gene panel and in both TGFβ receptors (**Fig. 1d, Supplementary Data 5**). TGFβ receptor mutations were again not identified in either distant or perilesional skin. To assess the potential lesion specific, non-germline significance of TGFβ receptor mutations, we interrogated the pyrosequencing analysis in depth from all of the samples containing normal matched tissue (**Supplementary Data 6**). We observed only 8 variant reads out of 1348

reads in total in 4 out of 25 matched normal sample reads. Three of these samples were from peri-lesional skin and likely reflect rare contaminating tumour cells. In comparison we observed 237 variant reads out of 1340 reads in the tumour samples. Employing Fisher's exact 2 sided tests to compare variant allele frequencies (VAFs) in matched samples, we determined that 17/25 of the TGFβ receptor mutations reached tumour specific VAF statistical significance confirming the lesion specific non-germline nature of these mutations (**Supplementary Data 6**).

TGFBR1 **and** ***TGFBR2*** **mutations are driver events in human cSCC**

Next we examined a further cohort of 30 primary cSCC samples with matched normal tissue (**Supplementary Table 4**) employing next generation WES (see Methods) and interrogated in detail *NOTCH1*, *NOTCH2*, *TP53*, *CDKN2A*, *HRAS*, *KRAS*, *NRAS*, *TGFBR1* and *TGFBR2* genes for mutational and copy number changes (**Fig. 2a and Supplementary Data 7**). We observed alterations in all of these genes with a similar frequency to that of our previous 454 pyrosequencing analysis. None of the mutational events were found in the matched normal samples and all except two of these were statistically significant (Fisher's exact *t*-test) (**Supplementary Data 8**). Importantly we observed changes in *TGFBR1* in 30% of the samples and changes in *TGFBR2* in 40% of the samples with a combined alteration in 53% of samples, confirming a frequent alteration of TGFβ receptor genes in cSCC. Copy number analysis also revealed that loss of heterozygosity (LOH) occurred in both *TGFBR1* and *TGFBR2* genes including in tumors with missense mutations in *TGFBR2* (**Fig. 2a, Supplementary Data 8**). Somatic single nucleotide variants (SNVs) of TGFβ receptors were detected in 30% of our samples consistent with our 454 pyrosequencing analysis and the recent sequencing analyses of two North American cSCC cohorts which, when combined,

158 detected TGFβ receptors protein altering SNVs in 15.7% of samples[16,17]. Given the high
159 mutational burden of cSCC, it is probable that many mutations identified will be passenger
160 mutations with no functional consequence for tumorigenesis. We investigated the potential
161 functional consequence of the mutations detected by WES employing MutsigCV[18] and
162 IntOgen analysis[19]. MutsigCV detected *TP53*, *CDKN2A*, *NOTCH1* and *NOTCH2* as significant
163 drivers but no *RAS* genes and IntOgen detected *TP53*, *CDKN2A NOTCH1* and *HRAS* as
164 significant drivers but did not identify *NOTCH2*, *KRAS* or *NRAS* (**Supplementary Data 9**).
165 Neither analysis detected *TGFBR1* or *TGFBR2* individually as significant drivers
166 (**Supplementary Data 9**), but IntOgen pathway analysis revealed TGFβ signaling as a
167 significantly altered signaling pathway (Oncodrive-fm functional impact bias, FM bias[19],
168 p=0.0019, **Supplementary Data 10**). We assessed the clonality of our candidate driver genes
169 using the ABSOLUTE algorithm[20]. WES data were of sufficient quality for 24/30 exomes and
170 ABSOLUTE analysis revealed purity and ploidy estimates ranging from 0.2-0.73 and 1.78-
171 5.79 respectively (**Supplementary Data 11**). ABSOLUTE clonality analysis indicated that all
172 *NOTCH1*, *CDKN2A*, and *RAS* mutations were clonal as were all bar one *TP53*, three *NOTCH2*
173 and one *TGFBR1* mutation which were subclonal (**Fig. 2b,c, Supplementary Data 12**).
174 Mutations present in nearly all tumor cells (clonal) would suggest early events and therefore
175 represent initiating "driver" genes as appears to be the case here for *NOTCH1*, *NOTCH2*,
176 *CDKN2A*, *HRAS*, *KRAS*, *TP53* and importantly both *TGFBR1* and *TGBFR2*.
177
178 Having established the likely driver event of mutation of *TGFBR1* and *TGFBR2* in our WES
179 data set we extended this analysis to include our samples assessed by targeted sequencing.
180 We first calculated average percentage VAFs for our candidate drivers and these ranged
181 from 48.7% for *CDKN2A* to 20% for *TGFBR1* (**Fig. 3a**). *TGFBR1* VAF was significantly lower

than that of *CDKN2A*, *TP53*, *HRAS*, *NOTCH1*, *TGFBR2* and *NOTCH2* but not *KRAS* and *NRAS* (**Fig. 3a, Supplementary Data 13**). *TGFBR2* VAF was only statistically significantly lower than *CDKN2A* and *TP53* but equivalent to *KRAS*, *NOTCH2* and *NRAS* (**Fig. 3a, Supplementary Data 13**). The VAFs of the TGFβ receptors are of a similar range to those observed in other cSCC driver genes. UV light is the major oncogenic stimulus of cSCC and the % of mutations conforming to a UV signature (C-T or G-A transitions) of our candidate drivers ranged from 79.7% in *CDKN2A* to 30.4% in *HRAS* (**Fig. 3b**) with mutations in both TGFβ receptor genes lying within this range. VAFs were statistically significantly higher for UV signature mutations for *NOTCH2*, *CDKN2A* and *TGFBR2* (**Supplementary Fig. 1a, Supplementary Data 14**). If these candidate genes represent potential driver genes then the mutational consequence should be predicted to change protein function. We classified these mutations as potentially damaging if they were predicted to be so by at least two of the four mutation function prediction programmes SIFT[21], PolyPhen-2[22], Provean[23] and Mutation Assessor[24] or were a splice site or PTC mutation (**Fig. 3c**). Damaging mutation rates ranged from 89% for *TP53* to 53.5% for *TGFBR1* (**Fig. 3c, Supplementary Data 15-23**) were statistically significantly higher for those with a UV signature for *NOTCH2*, *TGFBR2* and *TP53* (**Fig. 3d, Supplementary Data 24**) and damaging mutations had higher VAFs for *NOTCH2*, *CDKN2A*, *TGFBR2* and *NOTCH1* (**Supplementary Fig. 1b, Supplementary Data 25**). Together our data suggest that approximately 70% of *TGFBR2* and 50% of *TGFBR1* mutations will alter protein function with the potential to drive cSCC development. In its entirety our analysis conservatively estimates functionally relevant *TGFBR1* and *TGFBR2* mutations in ~10% and ~16% of samples respectively and therefore 20% of cSCC samples could harbour damaging TGFβ receptor mutations.

TGFβ receptor mutation inactivates canonical Smad signaling

Identified missense and nonsense mutations were found throughout the coding exons of both *TGFBR1* and *TGFBR2,* occurring in the extracellular and kinase domains of each protein (**Fig. 3e**). Structural analysis of the extracellular domains of TGFBR1 (**Supplementary Fig. 2**) and TGFBR2 (**Supplementary Fig. 3**) indicated mutations occur in, or in close proximity to, highly conserved disulphide bonds, ligand interaction motifs and/or receptor interaction motifs. These findings suggest significant potential for loss of function[25,26].

TGFβ signals via activation of a heterotetrameric complex of TGFBR2:TGFBR1, resulting in TGFBR1-kinase driven c-terminal phosphorylation of SMAD2 and SMAD3[27]. Once phosphorylated (PO_4), SMAD2 and SMAD3 form hetero-oligomeric complexes with the co-Smad SMAD4, accumulate in the nucleus and regulate gene expression of hundreds of target genes[28,29]. Activity of SMAD-dependent reporter gene constructs and steady state levels of SMAD2/3 c-terminal phosphorylation can be used as measures of canonical TGFβ signaling. To assess the functional consequence of these TGFβ receptor mutations we generated a panel of four TGFBR1 and five TGFBR2 mutant expression plasmids from mutations identified in our original targeted sequencing series. We assayed each mutant receptor for functional activity in transient transfection reporter gene assays. TGFBR1 expression plasmids were co-transfected into TGFBR1 null MEFS[30] and TGFBR2 expression plasmids were co-transfected into TGFBR2 null T47D breast cancer cells, in addition to the TGFβ responsive reporter construct SMAD7 Pomoter-luciferase[31] (**Fig. 4a and Fig. 4b respectively**). Wild type TGFβ receptor expression elevated reporter activity over empty vector controls, which was further elevated by TGFβ treatment (**Fig. 4a,b**). We confirmed this activity was dependent on intact SMAD binding elements in the SMAD7 promoter

(**Supplementary Fig. 4a,b**). The *TGFBR1* mutants H331R and W277C and all of the *TGFBR2* mutants (S474F, C486R, C96R, R2323W, A556T) failed to efficiently activate the reporter gene, despite similar levels of expression of the receptors, as assayed by western blotting (**Fig. 4a,b**). These findings indicate that mutation of *TGFBR1* and *TGFBR2* in cSCC frequently results in a loss of ability to activate canonical SMAD signaling. To demonstrate corollary of these findings in primary human tissue we then established conditions to monitor c-terminal PO_4-SMAD3 levels using a c-terminal Ser433/Ser435 PO_4-SMAD3 specific antibody in cSCC by immunohistochemistry (IHC) (**Supplementary Fig. 5**). We measured PO_4-SMAD3 activity in 8 primary tumors harbouring wild type receptors and 8 primary tumors harbouring mutant TGFβ receptors with a combined VAF of >20% (**Supplementary Data 26**). Wild type tumors exhibited readily detectable PO_4-SMAD3 activity whereas mutant tumors showed significantly reduced PO_4-SMAD3 activity (**Fig. 4c, Supplementary Fig. 6**), consistent with our observation that mutation of TGFβ receptors results in loss of canonical SMAD signaling activity. Both wild type and mutant tumors exhibited heterogeneity of staining consistent with our previous observations that cSCC is heterogenous in nature[6] and with the VAFs observed in mutant tumors.

Finally, we used primary human cSCC cell lines to assess whether TGFβ receptor mutation results in a loss of TGFβ signaling. Exogenous treatment of normal human keratinocytes (NHK) with TGFβ1 resulted in a dose dependent decrease in cell proliferation (**Fig. 4d**). The *TGFBR2* mutant harbouring cell lines SCCIC8 and SCCIC12 (**Supplementary Data 3**) failed to respond to exogenous TGFβ stimulation by either PO_4-SMAD activation (**Supplementary Fig. 7**) or by any effect on cell proliferation (**Fig. 4d**). Co-transfecting these *TGFBR2* mutant cells with either empty vector, or wild type TGFBR2 expression plasmids in addition to a GFP expression plasmid, we measured cell proliferation in real-time using Incucyte-Zoom™

imager over 6 days. Cell proliferation of the GFP^{+ve} cells indicated that cells expressing wild type TGFBR2 proliferated at a slower rate in the presence of exogenous TGFβ (**Fig. 4e**). The degree of inhibition was commensurate to the degree of restoration of SMAD activity as measured using the multimerised SMAD binding element reporter gene $CAGA_{12}$-Luciferase[32] (**Supplementary Fig. 7c,d**). These findings indicate that re-expression of wild-type TGFBR2 restores canonical TGFβ signaling and proliferative inhibition, confirming mutational loss of TGFβ tumor suppressive activity.

Matrix cells exhibit active TGFβ signaling

Given this potential aetiological loss of TGFβ signaling, we sought to identify sites of active TGFβ signaling in normal skin to gain insight into the cellular origin of cSCC RAF inhibitor induced lesions. PO_4-SMAD3 activity was barely detectable by IHC analysis in normal human epidermis (**Supplementary Fig. 8**) but showed strong immunoreactivity in the hair matrix zone of anagen hair follicles (**Fig. 5a, Supplementary Fig. 8**). PO_4-SMAD3 positivity was also detected in the hair matrix of anagen hair follicles in mouse back skin (**Fig. 5a**). In anagen, the hair follicle transit-amplifying (TA) cells are localized in the matrix and are positive for Sonic hedgehog (SHH)[11]. Elegant studies by the Blanpain group have demonstrated these cells are unable to act as a cell of origin for papilloma formation, even when both oncogenic *Kras* and *Tp53* were targeted[11]. This suggests that these PO_4-$SMAD3^{+ve}$ hair matrix cells are unlikely to be the cell of origin for the rapid cSCC observed in humans following RAF inhibitor treatment. To investigate this in the mouse, we tested if *Tgfbr1* deletion could permit the transformation of TA cells. RAF inhibitors stimulate paradoxical activation of the MAPK pathway in cells with wild-type BRAF harbouring upstream pathway activation, via mechanisms such as: up-regulated receptor tyrosine kinases, oncogenic RAS via RAF dimer

formation[33-35], or relief of inhibitory auto-phosphorylation[36]. Circumventing pharmacological enhancement of MAPK signaling in the presence of mutated *RAS*, we modelled hyperactivation of the MAPK pathway in the SHH^{+ve} compartment by targeting downstream oncogenic $Braf^{V600E}$ and oncogenic activation of $Kras^{G12D}$. We crossed our previously described *LSL-*$Braf^{V600E}$ mice[37], which allow inducible expression of $Braf^{V600E}$ from the endogenous *Braf* gene, with the $ShhCRE^{ER}$ strain[38]. This permits tamoxifen inducible activation of the Cre recombinase in SHH^{+ve} cells. To assess the role of TGFβ signaling in the SHH^{+ve} cells, we then crossed these animals with $Tgfbr1^{fl}$ mice[30] (**Supplementary Fig. 9a,b**). No tumors formed in the skin of $ShhCRE^{ER}$ $Braf^{V600E}$ and $ShhCRE^{ER}$ $Braf^{V600E}$ $Tgfbr1^{fl/+}$ mice (**Fig. 5b, Supplementary Fig. 10a,b**). A small percentage of $ShhCRE^{ER}$ $Braf^{V600E}$ $Tgfbr1^{fl/fl}$ mice developed minimally proliferative papillomatous lesions (as evidenced by low level BrdU staining) mainly in the lips, but only at long latency (**Fig. 5b, Supplementary Fig. 10c**). No mice developed cSCC. Mice failed to develop any skin lesions following oncogenic activation of $Kras^{G12D}$ with or without deletion of *Tgfbr1* in this cell compartment (**Fig. 5c**). Together these studies indicate that the SHH^{+ve} cells are unlikely to be the cell of origin for either rapid onset vemurafenib-induced cSCC, or sporadic cSCC.

TGFβ signaling is active in telogen bulge stem cells

Approximately 90% of human hair follicles are present in the anagen phase of the hair cycle with the remaining 10% existing in catagen or the resting telogen phase. Analysis of human telogen hair follicles revealed highly localised PO_4-SMAD3 staining in the bulge stem cells, characterised in part by KERATIN 15 staining (**Fig. 6a**). This pattern was recapitulated in mouse telogen hair follicles (**Fig. 6b**), characterised by the expression of the stem cell marker LGR5[39]. To investigate further, we used the *Lgr5-EGFP-Ires-CREERT2* knockin mouse

(hereafter termed *Lgr5CRE^{ER}*), where the endogenous *Lgr5* promoter controls expression of enhanced green fluorescent protein (EGFP) and the CREERT2 fusion protein[40]. IHC analysis for GFP revealed a staining pattern similar of that observed for PO_4-SMAD3 (**Fig. 6c**). Furthermore, co-immunofluorescence revealed LGR5^{+ve} cells (stained for EGFP) are highly enriched for both PO_4-SMAD3 and TGFBR1 (**Fig. 6d and Supplementary Fig. 11**).

Recent studies indicate that the dermal papilla may provide a source of TGFβ2, activating SMAD signaling in overlying hair germ stem cells[41]. We sorted epithelial EGFP positive LGR5^{+ve} stem cells from murine back skin. Quantitative reverse-transcriptase PCR (Q-RTPCR) analysis revealed LGR5^{+ve} cells express enhanced levels of *Tgfbr1, Tgfb1* and *Tgfb3* mRNA when compared to LGR5^{-ve} cells, with negligible amounts of *Tgfb2* (**Fig. 6e**). Expression of *Tgfbr2* was readily detected in GFP^{+ve} and GFP^{-ve} compartments (**Fig. 6e**). This indicates enriched autocrine TGFβ signaling in the LGR5^{+ve} compartment. We observed high levels of the TGFβ target gene *Smad7*[42] in LGR5^{+ve} cells (**Fig. 6e**). Together these findings indicate that autocrine TGFβ signaling is highly localised to the LGR5^{+ve} hair follicle bulge stem cells in the mouse, and the KERATIN 15^{+ve} hair follicle bulge stem cells in humans, and that this cell compartment may give rise to both vemurafenib-induced and sporadic cSCC.

Rapid cSCC formation from Lgr5^{+ve} stem cells

To investigate the consequence of hyperactivation of the MAPK pathway coupled with ablation of TGFβ signaling in LGR5^{+ve} stem cells we crossed the *Lgr5CRE^{ER}* mice with the *LSL-Braf^{V600E}* mice (**Supplementary Fig. 9c**), or *LSL-Kras^{G12D}* mice and *Tgfbr1^{fl}* mice (**Supplementary Fig. 9d**). Loss of TGFβ signaling alone was not sufficient to initiate tumorigenesis (**Fig. 7a**). Targeted activation of BRAF to LGR5^{+ve} cells resulted in decreased

survival, with all mice euthanized 300-days post induction of the transgene by injection of tamoxifen (Median survival 276 days). Whilst 6 out of 14 mice succumbed to adrenal tumors, 50% of these mice presented with papillomas consistent with LGR5 expression in murine skin (**Fig. 7a,c**). However, the long latency period suggests *Braf* mutation requires additional events to facilitate papilloma development. The combined targeted inactivation of one allele of *Tgfbr1* reduced survival (median survival 231 days) and enhanced both the number of mice with skin lesions, and the number of lesions per mouse (**Fig. 7a,c and Supplementary Fig. 12a**). Inactivation of both *Tgfbr1* alleles significantly increased the numbers of tumor per mouse and dramatically shortened both skin tumor free survival (all mice developing skin lesions within 63 days of induction) and overall survival (median survival 51 days) (**Fig. 7a,c and Supplementary Fig. 12a**). Phenotypically these lesions appeared as differentiated papillomas in *Tgfbr1* wild-type and heterozygous mice (**Fig. 7c-e and Supplementary Fig. 12b).** Remarkably, in the homozygous $Tgfbr1^{fl/fl}$ mice tumors appeared as ulcerative cSCC (**Fig. 7c and Supplementary Fig. 12b)**. Elegant work by the Blanpain and Jensen laboratories[10,11] have shown when *Kras* is targeted to skin stem cells, there is long latency to papilloma formation (similar to the $Braf^{V600E}$ allele described here) and most of these lesions form around areas associated with wounding. Targeted activation of *Kras* alone mainly failed to produce skin lesions, however, when we targeted inactivation of both alleles of *Tgfbr1* and the $Kras^{G12D}$ mutation to the $LGR5^{+ve}$ compartment, mice developed rapid cSCC with kinetics comparable to $Braf^{V600E}$ mice (**Fig. 7b,c**). Additionally, KERATIN1 (**Fig. 7d**) and KERATIN 5 staining (**Fig. 7e**) revealed that cSCC lesions in both the *Braf* and *Kras* mice are poorly differentiated cSCC. Importantly these lesions were highly proliferative (**Supplementary Fig. 12c**) and never progressed via a papillomatous stage, recapitulating the rapid cSCC onset observed in humans[12,13]. PO_4-SMAD3 activity exhibited a

dose dependent reduction in tumors isolated from these mice, indicating loss of TGFβ signaling (**Supplementary Fig. 12d,e**). Q-RTPCR analysis of these tumors revealed loss of *Tgfbr1* expression (**Supplementary Fig. 12f**) without any significant change in ligand mRNA expression (**Supplementary Fig. 13**).

Skin tissue compartmentalization has been recently proposed as a mechanism involved in tissue maintenance[10]. To test if *Tgfbr1* deletion perturbed such compartmentalization, we lineage traced LGR5^{+ve} cells by intercrossing *Lgr5Cre^{ER}* with the *Rosa$^{LSL-RFP}$* reporter mice (**Supplementary Fig. 9e**). We observed that RFP positive cells were confined to the hair follicle[39] and were never detected in the sebaceous gland, or interfollicular epidermis regions of *Lgr5Cre^{ER} Braf^{V600E}*, or *Lgr5Cre^{ER} Braf^{V600E} Tgfbr1$^{fl/+}$* mice, at early time points post induction (**Supplementary Fig. 14**). The cSCC arising within *Lgr5Cre^{ER} Braf^{V600E} Tgfbr1$^{fl/fl}$* mice were fully recombined and RFP positive. In the normal skin comparator for these tumours, but also at earlier time points, the LGR5^{+ve} cells and their progeny were localised in their normal compartment (**Supplementary Fig. 14**). These results indicate that perturbation of TGFβ signaling is insufficient to disrupt compartmentalization, but acts as a tumour suppressor in LGR5^{+ve} stem cells.

Given the infrequent coincident activation of *RAS* genes and mutational inactivation of TGFβ receptors in sporadic cSCC we finally sought to model this disease by inactivating TP53 function coupled with deletion of *Tgfbr1* in LGR5^{+ve} cells (**Supplementary Fig. 9f**). Knockin of mutant *Tp53* (R172H) coupled with deletion of the wild type allele had no discernible phenotype (**Fig. 8a**). Heterozygous knockin or deletion of *Tp53* coupled with homozygous deletion of *Tgfbr1*resulted in the emergence of skin tumours in a few mice (30% and 20%

respectively) with long latency. Combined knockin of mutant *Tp53* with deletion of the wild type allele of *Tp53* coupled with deletion of *Tgfbr1*resulted in skin tumor development in 81% of mice with increased tumor number at a shorter latency (**Fig. 8a,b**). These tumors exhibited loss of differentiation expressing low levels of KERATIN 1 and higher levels of KERATIN 5 (**Fig. 8c**).

Discussion

Recent studies have revealed an exceptionally high mutation burden (50 mutations per megabase of DNA[6]) in cSCC[6,16,17]. This rate is second only to that of the commonest skin malignancy basal cell carcinoma[43]. This translates to potentially thousands of mutations per tumor, providing a particular challenge in identifying driver mutations. This challenge is further compounded by varying efficiencies in deep sequencing technologies and profound tumor heterogeneity[2,6,44,45]. Our studies here reveal that targeted deep sequencing using fluidigm PCR amplification and Roche 454 pyrosequencing can provide a robust platform to identify mutations in *NOTCH1*, *NOTCH2*[6],*TGFBR1* and *TGFBR2* genes. This approach has also implicated alterations of *NOTCH*, *TP53* and *RAS* in cSCC tumor development[6,46]. We further these studies by revealing mutation of TGFβ receptors in 43% of sporadic human cSCC and 28% of vemurafenib-induced skin lesions (**Fig. 1**). The prevalent tumor initiating event in cSCC is UV-induced damage, which manifests as C-T and G-A transitions[39]. Approximately 68% of all nucleotide changes observed in our cSCC samples present with this signature[6]. Analysis of mutational signatures in TGFβ receptors reveals that 42% conform to a UV signature (**Fig. 3b, Supplementary Data 13**). This figure increases to 56.1% when scored as possibly damaging events via protein function prediction programmes (**Fig. 3d,**

Supplementary Data 24). This indicates that UV damage may also be responsible for inactivation of TGFβ receptors. Mutation prediction programmes scored 53.5% of *TGFBR1* and 71.1% of *TGFBR2* receptor mutants as damaging indicating that approximately 20% of cSCC harbour TGFβ receptor inactivation (**Supplementary Data 15-16, Fig. 3c**). Subsequent functional analysis of 4 TGFBR1 mutants and 5 TGFBR2 mutants indicated that half of the TGFBR1 mutants and all five TGFBR2 mutants were loss of function for canonical Smad signaling and that tumors harbouring TGFβ receptor mutations had reduced PO_4-SMAD3 activity (**Fig. 4**). Restoration of TGFBR2 expression to TGFBR2 null cell lines restricted cell proliferation (**Fig. 4**). Taken together these findings indicate that loss of TGFβ tumour suppressor function is a common event in cSCC.

The assessment of VAFs provides an indication of the clonality of tumors and aids the potential identification of early driver mutationss during tumor development[2]. We ranked mutational events by potential order of occurrence in the 7 genes we have previsouly implicated in cSCC development and TGFβ receptors by measurement of VAF (**Supplementary Data 15-16**). These analyses indicate that potentially damaging mutations in TGFBR1 occur early in 25% of tumors harbouring these mutations and in 42% of tumors harbouring potentially damaging TGFBR2 mutations. Although this analysis is limited to the 9 genes studied in-depth here (but importantly including *NOTCH* genes previously identified as gatekeeper mutations in cSCC[6]), 11 samples exhibited TGFβ receptor mutations with the highest VAF indicating that this could be an initiating event in the development of cSCC. Strong support for this hypothesis comes from ABSOLUTE clonality analysis of our WES samples which revealed that 7/8 TGFβ receptor mutations were clonal and represent probable driver events in these lesions.

Several of our samples display VAFs of 10-20% for the TGFβ receptors which is not too dissimilar to the VAFs of the other known cSCC tumor suppressors studied here and likely reflects the heterogeneous nature of cSCC. It is however an intriguing possibility that in some cases low TGFβ receptor VAF may reflect spontaneous regression of TGFβ receptors mutant clones as observed in multiple self-healing squamous epithelioma (MSSE) patients who harbour germline mutations in *TGFBR1*[47]. TGFβ signaling has been demonstrated to play both positive and negative roles in cSCC development in various mouse models[48] acting to limit tumor cell proliferation but also to promote tumor initiating capacity and drug resistance[49]. Effects are dependent on the timing of aberrant TGFβ signaling and the cooperating oncogenic driving events (reviewed in[48,50-52]). We provide evidence that a dose-dependent loss of TGFβ signaling drives tumor progression - emphasising its role as a major tumor suppressor in the skin. Although the cell of origin in cSCC in humans remains poorly defined[3], our observations indicate that tumors can initiate efficiently and rapidly from LGR5^{+ve} stem cells compared to TA cells, and mutational modulation of two signaling pathways within this cellular compartment is sufficient to drive rapid progression directly to carcinoma, without the need for protracted tumour evolution. The kinetics of this event mimic exactly that observed during development of cutaneous lesions in RAF inhibitor treated patients[12,13]. Intriguingly this rapid process requires MAPK pathway activation as targeted intereference with TP53 fu nction coupled with *Tgfbr1* loss results in the development of skin tumours with long latency. Importantly our studies revealed highly localised TGFβ signaling in KERATIN 15^{+ve} bulge stem cells in human telogen hair follicles, mirrored exquisitly the location of specific autocrine TGFβ signaling activity identified in LGR5^{+ve} bulge stem cells of murine telogen hair follicles. It has been proposed that stem cell

quiescence acts as a tumor suppresive mechanism in murine skin and that LGR5^{+ve} stem cells are refractory to oncogenic transformation[53]. Our data clearly indicate that oncogenic activation of the RAS/RAF/MAPK pathway, or TP*53* modulation, coupled with loss of TGFβ signaling, is capable of leading to tumor development from this compartment. As we demonstrate that mutational inactivation of TGFβ receptors is a frequent event in human cSCC, and that TGFβ signaling is highly localised to stem cells in normal skin, we propose that these cells represent a cell of origin for human cSCC. It remains possible that loss of TGFβ signaling may also contribute to cSCC development from other cell compartments in the skin and this warrants further investigation.

Our data, both in human and mice, indicate that TGFβ signaling inactivation can be an initiating event in sporadic cSCC. This is clearly the case in MSSE where germline loss of function mutations in *TGFBR1* have been identified as the underlying genetic lesion[47]. We speculate that activation of the RAS/RAF/MAPK pathway, or p53 modulation, may be a cooperating event in the development of this disease and that these tumors may originate from the bulge stem cell compartment. TGFβ signaling inactivation may also occur following the acquisition of other driving mutational events and act as a limiting factor for tumor development. Intriguingly, initial clinical trials targeting systemic TGFβ inhibition with GC1008 (a pan-TGFβ neutralising antibody) have also reported the occurrence of spontaneous cSCC as a side effect[54]. This provides further compelling support for the tumor suppressive role of TGFβ in skin carcinogenesis.

Methods

Samples. Ethical approval for this investigation was obtained from the East London and City Health Authority and the Tayside Tissue bank local ethics committee and the study was conducted according to the Declaration of Helsinki Principles. All patients participating in this study were from dermatology and plastic surgery units in the UK and all provided written, informed consent. Punch biopsies of cSCC tissue were collected and processed as previously reported[6]. Normal human keratinocytes were isolated from normal skin samples according to previously published protocols[55]. Human tumor cell lines SCCIC1, SCCIC4, SCCIC8, SCCIC15, SCCIC12, SCCIC18, SCCIC19, SCCIC21, SCCT1, SCCT2, SCCT6, SCCT8, PM1, MET1, MET4, SCCT9, SCCT10, SCCT11, RDEBSCC2, RDEBSCC3, RDEBSCC4 and NTERT cells were established by our laboratories and were cultured as described[15]. TGFBR1 null MEFs[30] and T47D cells (ATCC) were maintained in DMEM and RPMI supplemented with 10% FCS respectively. Mycoplasma contamination checks were carried out on all cultures as routine and all lines were confirmed mycoplasma negative.

454 sequencing. *TGFBR1* and *TGFBR2* primers were designed and validated by Fluidigm (Fluidigm Corporation, San Francisco, CA) as per recommended guidelines for Roche Titanium sequencing (Roche, Mannheim, Germany). Primers for *NOTCH1*, *NOTCH2*, *TP53*, *CDKN2A*, *HRAS*, *KRAS* and *NRAS* were previously described[6] and all primer sequences are listed in Supplementary Data 27. Each primer included sample-specific Fluidigm 454 barcode primer and adapter sequences. Sequencing was performed in the same manner as our previous study[56]. Briefly for thermal cycling a Fluidigm FC1 Cycler was used. The libraries were normalized and pooled prior to purification using Agencourt AMPure XP system (Beckman, UK). Library components were clonally amplified utilising the GSJunior emPCR

Lib-A Kit (Roche) by inputting 1 molecule of library DNA per capture bead. Pyrosequencing was done using the GS Junior system (Roche/454 Life Sciences).

454 variant analyses. Variant analysis was performed as previously described[6]. Briefly, reads were mapped to the hg19 build of the human genome using LASTZ via the public GALAXY instance and filtered to exclude those mapping to <100 loci using tools available through GALAXY.

Coding Variants and splice site detection. Pileup files were generated and filtered using SAMTools[57]. Variants present in a single read or less than 10% of the total reads were excluded using a custom java program available from https://github.com/mattsouth/laszt-variant-filter (last accessed 6th May 2013). Coding variants were called against the RefSeq gene list using the amino acid tool via the public GALAXY instance. Variants present in <3 reads were excluded. Variants present in >1 independent sample and adjacent to a homopolymer >3 bases were excluded unless present in COSMIC[58]. Variants present in >30 samples were excluded unless present in COSMIC. All variants present in the exome variant server database (http://evs.gs.washington.edu/EVS/) were excluded unless present in COSMIC. Splice sites were called from the pileup variant list if present in >4 reads and within 2 bases of Refseq coding sequence using Excel (Microsoft Inc., CA).

Whole exome sequencing data analysis. 20 previously published cSCC whole exomes[6] were re-analysed with the addition of 10 new cSCC whole exomes with the overall mean coverage of 63x (Supplementary Table 4), using a previous pipeline[59]. SNVs and short indels were identified using the Strelka pipeline[60] with a minimum coverage of 10 reads at the targeted

sites. Annotation of somatic variants was performed using the Oncotator tool[61]. Mutations in our targeted genes were further identified across the 30 cSCC WES samples.

Copy number analysis using WES data. Two independent approaches were applied. First, to generate SNP and indel variant genotyping information, the tumor-normal pair was processed together against the reference genome using the VarScan2 germline variants calling method mpileup2cns[62]. The minimum coverage for identified sites was 10 reads for both tumor and normal. Next the logR and BAF (B-allele frequency) files were created based on the tumor-normal pair genotyping information, with the depth information normalized by dividing the depth of each variant by the median depth across all variants. The ASCAT R packages[63] were then used to perform allele-specific copy number analysis to identify copy number aberrations (CNA) and loss-of-heterozygosity (LOH) regions. The second approach was based on numbers of reads aligned to each exon between the tumor and normal pair. VarScan2 copy number calling method was firstly applied. Raw copy number calls were adjusted as previously reported[64]. Finally results from the two approaches were cross-compared to produce the final CNA and acquired uniparental disomy (aUPD) calls for targeted genes.

Identification of potential cancer drivers and significantly mutated pathways. Based on all mutations identified from the 30 cSCC WES dataset, we used the IntOGen platform[19] to identify significantly mutated genes and pathways, based on the significance (*p*-value) of the FM bias (i.e., the bias toward the accumulation of mutations with high functional impact). The significantly mutated signaling pathways (based on the IntOGen Oncodrive-fm functional impact bias, FM bias $p < 0.05$)) were further selected (**Supplementary Data 10**).

MutsigCV[18] was also used to detect significant genes with point mutations above the background mutation rate.

Estimating the clonality of mutations. For the somatic mutations of *TGFBR1/2*, *TP53*, *CDKN2A*, *NOTCH1/2* and *RAS* genes identified by WES (**Supplementary Data 7**), we further classified them as clonal or subclonal on the basis of the posterior probability that the cancer cell fraction (CCF) exceeded 0.95 using ABSOLUTE[20]. Numbers of reads supporting the reference and alternative alleles were extracted, and the copy number segmentation files were generated based on the DNAcopy CBS segments using WES data. Mutations with the somatic clonal probability > 0.5 were classified as clonal with high confidence. Those mutations with clonal probability > 0.25 but with very small subclonal probability scores were also called clonal (**Supplementary Data 12**). Tumor purity and ploidy were also estimated (**Supplementary Data 11**). For samples with *TGFBR1/2* mutations, CCFs for *TGFBR1/2* were further compared to those for other genes to determine the clonality orders.

Functional prediction of mutations. A combination of four approaches were used to predict the functional impact of identified mutations by targeted sequencing, (i) SIFT[21], which uses sequence homology and protein conservation to predict the effects of all possible substitutions at each position in the protein sequence; (ii) PolyPhen-2[22], which predicts possible functional impact of an amino acid substitution on the structure and function level using physical and comparative considerations; (iii) Provean[23], which predicts the damaging effects of SNVs and indels using a versatile alignment-based score; and (iv) Mutation Assessor[24], which measures the functional impact scores for amino acid residue changes

using evolutionary conservation patterns derived from aligned families and sub-families of sequence homologs within and between species. Mutations predicted as functional damaging by at least two of the four approaches were classified being potentially damaging/deleterious.

***In Vivo* analyses.** All experiments were performed under the UK Home Office guidelines. Mice were segregating for C57BL6J and S129 background. Alleles used throughout this study were: *Lgr5-cre-ER^{T240}, ShhCre^{ER38}, Braf^{V600E37}, Kras^{G12D65} , Tgfbr1^{fl30} and Rosa$^{LSL-RFP66}$*. A mix of males and females were used. Recombination in the *Lgr5-cre-ER^{T2}* mouse model was induced with 1 intraperitoneal (IP) injection of 3 mg Tamoxifen (Sigma) followed by 1 injection of 2 mg Tamoxifen for 3 days. Mice were induced post 7 weeks of age. Recombination in the *ShhCre^{ER}* mouse model was induced with 1 IP injection of 2.5 mg Tamoxifen. Mice were induced post 28 days of age. For proliferation analysis mice were injected with 250 µl of BrdU (Amersham Biosciences) 2 hours before being sacrificed.

FACS analysis. Epidermis was prepared as previously described[67]. Briefly, fat was scraped from the mouse back and left at 37°C in a dish (dermis down) in 0.25% of Trypsin/EDTA (Invitrogen) for 90 min. Epidermis was removed using a scalpel and dissociated by pipetting. Cells were filtered through a 40 µm strainer, centrifuged at 250g for 5 min and washed with PE (PBS/EDTA). Cells were washed with 0.1% BSA/PE, centrifuged at 250g for 5 min and used for Lgr5-GFP sorting.

588 **Immunohistochemistry.** Immunohistochemistry (IHC) was performed on formalin-fixed skin
589 sections. Standard IHC techniques were used throughout this study. Primary antibodies
590 were as follows: TGFBR1 (Santa Cruz, V22, 1:100), PO_4-SMAD3 (Abcam, EP823Y, (52903),
591 1:50), GFP (Abgent, 168AT1211, 1:100), KERATIN1 (Covance, AF109, 1:1000), KERATIN 5
592 (Covance, AF138, 1:4000), KERATIN 15 (Abcam, 80522 (LHK15), 1:1000), KI67 (Thermo, RM-
593 9106-S), BrdU (BD Biosciences, 347580, 1:200;). Mouse PO_4-SMAD3 score was performed in
594 a blinded fashion. For each antibody, staining was performed on at least 3 mice of each
595 genotype and at least six sections of normal human skin. Representative images are shown
596 for each staining. PO_4-SMAD3 antibody was optimised for IHC use using FFPE embedded
597 SCCIC4 cells treated with and without recombinant TGFβ1 or the TGFBR1 kinase inhibitor
598 SB-431542[68] (**Supplementary Figure 5**). PO_4-SMAD3 IHC scoring was performed in a blinded
599 manner using the histoscore method.

600

601 **RNA isolation and quantitative PCR** RNA was isolated using a Qiagen RNeasy Mini Kit
602 (Qiagen, Crawly, West Sussex, UK) according to the manufacturer's instructions. DNA-free
603 (Ambion/Applied Biosystems, Warrington, UK) was used to remove genomic DNA
604 contamination according to the manufacturer's instructions. 1ug of RNA was reverse
605 transcribed to cDNA using a DyNAmo SYBR Green 2-step qPCR kit (Finnzymes, Espoo,
606 Finland) in a reaction volume of 20 µl. GAPDH was used to normalize for differences in RNA
607 input.

608

609 **qRT-PCR primers**. qRT–PCR primers were as follows. m*Tgfbr1* F-TGCCATAACCGCACTGTCA,
610 m*Tgfbr1* R-AATGAAAGGGCGATCTAGTGATG, m*Tgfbr2* F-CCGGAA GTTCTAGAATCCAG,

m*Tgfbr2* R-TAATCCTTCACTTCTCCCAC, m*Tgfb1* F-AGCCCGAAGCGGACTACTAT, m*Tgfb1* R-TTCCACATGTTGCTCCACAC, m*Tgfb2* F-TTTAAGAGGGATCTTGGATGGA, m*Tgfb2* R-AGAATGGTCAGTGGTTCCAGAT, m*Tgfb3* F-CGCACAGAGCAGAGAATTGA, m*Tgfb3* R-GTGACATGGACAGTGGATGC, m*Smad7* F-TCAAGAGGCTGTGTTGCTGT, m*Smad7* R-TGGGTATCTGGAGTAAGGAGGA, m*Gapdh* F-GAAGGCCGGGGCCCACTTGA, m*Gapdh* R-CTGGGTGGCAGTGATGGCATGG

Western Blotting. Cells were lysed directly in 4xSDS sample buffer at 60-80% confluence. Lysates were subjected to standard SDS-PAGE. Bands were detected using enhanced chemi-luminescence solution (ECL, Amersham). Secondary antibodies used throughout: HRP-conjugated polyclonal goat anti-mouse Ig (Dako, P0448, 1:2000), HRP-conjugated polyclonal goat anti-rabbit Ig (Dako, P0260, 1:2000). Primary antibodies were PO_4-SMAD3 (Abcam, 52903, 1:1000), SMAD3 (Cell Signaling, 9523, 1:1000), TGFBR1 (Santa Cruz, 398 (V22), 1:500), TGFBR2 (Santa Cruz, 17792, (E6), 1:500). For TGFBR2 western blots, lysates were prepared directly from transfected cells using the Dual-luciferase cell lysis buffer (Promega). For TGFBR1 western blots, parallel transfections to the luciferase assays were performed and samples were lysed directly in 4xSDS sample buffer. Original uncropped western blot scans are also provided (Supplementary Figure 15).

Plasmids. The full-length wild type human TGFBR1 and pathogenic mutants, amplified with *BglII/NotI* restriction sites, were shuttled into pCMV5 mammalian cell expression vectors onto the *BamHI/NotI* sites. The full-length wild type human TGFBR2 and pathogenic mutants were sub-cloned into pCMV5 using the *BamHI/NotI* restriction sites. Site-directed

mutagenesis was carried out using the QuickChange method (Stratagene) but substituting the Taq with KOD Hot Start DNA polymerase (Novagen). All DNA constructs were verified by DNA sequencing (by the DNA Sequencing Service at University of Dundee; www.dnaseq.co.uk). GFP expression plasmid was from Amaxa.

Transient transfection analysis. All transfections were performed in 24-well format in biological triplicate using LipofectAMINE 2000 (Invitrogen, Carlsbad, CA) according to manufacturer's instructions. Cells were transfected overnight with 100ng of reporter gene (SMAD7 Promoter-Luciferase or $CAGA_{12}$-Luciferase) and 10ng of internal Renilla-Luciferase control (pRL-TK, E2241, Promega) with empty vector (pCMV5, 211175, Stratagene), wild type or mutant TGFβ receptor plasmids (range 150-300ng). Recombinant human TGFβ1 (Peprotech) was dissolved in 4mM HCL/1mg/ml BSA and used at final concentration of 5ng/ml and cells were treated for 4 hours prior to harvest. Luciferase activities were measured using the Dual Luciferase assay (Promega) and firefly luciferase activity was normalised to renilla luciferase activity.

Cell proliferation assays. Cells were seeded at a density of 500-1000 cells/well of 96-well plates in keratinocyte media (RM^+) without growth factors and incubated overnight. Cells were fed 50µl of medium supplemented with treatment and controls every 2 days until harvest. All cultures were performed in sextuplet (n=6). Cells were assayed for proliferation using the CellTitreGlo™ Luminescent Cell Viability assay (NHKs) as per the manufacturer's instructions (Promega, UK - Luminesence was measured on a Berthold Orion II microplate luminometer) or IncucyteZoom™ Live cell imager.

Data availability

The whole exome sequencing data for the 30 samples have been deposited in the European Genome-phenome Archive (EGA) under accession code EGAS00001001892. The authors declare that all other relevant data supporting the findings of this study are available within the article and its supplementary information files. Additional information can be obtained from the corresponding authors (GJI and OJS).

References

1. Greaves, M. & Maley, C.C. Clonal evolution in cancer. *Nature* **481**, 306-13 (2012).
2. Vogelstein, B. et al. Cancer genome landscapes. *Science* **339**, 1546-58 (2013).
3. Blanpain, C. Tracing the cellular origin of cancer. *Nat Cell Biol* **15**, 126-34 (2013).
4. Barker, N. et al. Crypt stem cells as the cells-of-origin of intestinal cancer. *Nature* **457**, 608-11 (2009).
5. Schwitalla, S. et al. Intestinal tumorigenesis initiated by dedifferentiation and acquisition of stem-cell-like properties. *Cell* **152**, 25-38 (2013).
6. South, A.P. et al. NOTCH1 mutations occur early during cutaneous squamous cell carcinogenesis. *J Invest Dermatol* **134**, 2630-8 (2014).
7. Stahl, P.L. et al. Sun-induced nonsynonymous p53 mutations are extensively accumulated and tolerated in normal appearing human skin. *J Invest Dermatol* **131**, 504-8 (2011).
8. Martincorena, I. et al. Tumor evolution. High burden and pervasive positive selection of somatic mutations in normal human skin. *Science* **348**, 880-6 (2015).
9. Nelson, M.A., Futscher, B.W., Kinsella, T., Wymer, J. & Bowden, G.T. Detection of mutant Ha-ras genes in chemically initiated mouse skin epidermis before the development of benign tumors. *Proc Natl Acad Sci U S A* **89**, 6398-402 (1992).
10. Page, M.E., Lombard, P., Ng, F., Gottgens, B. & Jensen, K.B. The epidermis comprises autonomous compartments maintained by distinct stem cell populations. *Cell Stem Cell* **13**, 471-82 (2013).
11. Lapouge, G. et al. Identifying the cellular origin of squamous skin tumors. *Proc Natl Acad Sci U S A* **108**, 7431-6 (2011).
12. Oberholzer, P.A. et al. RAS mutations are associated with the development of cutaneous squamous cell tumors in patients treated with RAF inhibitors. *J Clin Oncol* **30**, 316-21 (2012).
13. Su, F. et al. RAS mutations in cutaneous squamous-cell carcinomas in patients treated with BRAF inhibitors. *N Engl J Med* **366**, 207-15 (2012).
14. Arnault, J.P. et al. Skin tumors induced by sorafenib; paradoxic RAS-RAF pathway activation and oncogenic mutations of HRAS, TP53, and TGFBR1. *Clin Cancer Res* **18**, 263-72 (2012).

15. Purdie, K.J., Pourreyron, C. & South, A.P. Isolation and culture of squamous cell carcinoma lines. *Methods Mol Biol* **731**, 151-9 (2011).
16. Pickering, C.R. et al. Mutational landscape of aggressive cutaneous squamous cell carcinoma. *Clinical cancer research : an official journal of the American Association for Cancer Research* **20**, 6582-92 (2014).
17. Lee, C.S. et al. Recurrent point mutations in the kinetochore gene KNSTRN in cutaneous squamous cell carcinoma. *Nat Genet* **46**, 1060-2 (2014).
18. Lawrence, M.S. et al. Mutational heterogeneity in cancer and the search for new cancer-associated genes. *Nature* **499**, 214-8 (2013).
19. Gonzalez-Perez, A. et al. IntOGen-mutations identifies cancer drivers across tumor types. *Nature methods* **10**, 1081-2 (2013).
20. Carter, S.L. et al. Absolute quantification of somatic DNA alterations in human cancer. *Nature biotechnology* **30**, 413-21 (2012).
21. Kumar, P., Henikoff, S. & Ng, P.C. Predicting the effects of coding non-synonymous variants on protein function using the SIFT algorithm. *Nature protocols* **4**, 1073-81 (2009).
22. Adzhubei, I.A. et al. A method and server for predicting damaging missense mutations. *Nature methods* **7**, 248-9 (2010).
23. Choi, Y., Sims, G.E., Murphy, S., Miller, J.R. & Chan, A.P. Predicting the functional effect of amino acid substitutions and indels. *PLoS One* **7**, e46688 (2012).
24. Reva, B., Antipin, Y. & Sander, C. Predicting the functional impact of protein mutations: application to cancer genomics. *Nucleic acids research* **39**, e118 (2011).
25. Groppe, J. et al. Cooperative assembly of TGF-beta superfamily signaling complexes is mediated by two disparate mechanisms and distinct modes of receptor binding. *Mol Cell* **29**, 157-68 (2008).
26. De Crescenzo, G. et al. Three key residues underlie the differential affinity of the TGFbeta isoforms for the TGFbeta type II receptor. *J Mol Biol* **355**, 47-62 (2006).
27. Massague, J. TGFbeta signalling in context. *Nat Rev Mol Cell Biol* **13**, 616-30 (2012).
28. Ross, S. & Hill, C.S. How the Smads regulate transcription. *Int J Biochem Cell Biol* **40**, 383-408 (2008).
29. Massague, J., Seoane, J. & Wotton, D. Smad transcription factors. *Genes Dev* **19**, 2783-810 (2005).
30. Larsson, J. et al. Abnormal angiogenesis but intact hematopoietic potential in TGF-beta type I receptor-deficient mice. *EMBO J* **20**, 1663-73 (2001).
31. Denissova, N.G., Pouponnot, C., Long, J., He, D. & Liu, F. Transforming growth factor beta -inducible independent binding of SMAD to the Smad7 promoter. *Proc Natl Acad Sci U S A* **97**, 6397-402 (2000).
32. Dennler, S. et al. Direct binding of Smad3 and Smad4 to critical TGF beta-inducible elements in the promoter of human plasminogen activator inhibitor-type 1 gene. *EMBO J* **17**, 3091-100 (1998).
33. Heidorn, S.J. et al. Kinase-dead BRAF and oncogenic RAS cooperate to drive tumor progression through CRAF. *Cell* **140**, 209-21 (2010).
34. Poulikakos, P.I., Zhang, C., Bollag, G., Shokat, K.M. & Rosen, N. RAF inhibitors transactivate RAF dimers and ERK signalling in cells with wild-type BRAF. *Nature* **464**, 427-30 (2010).
35. Hatzivassiliou, G. et al. RAF inhibitors prime wild-type RAF to activate the MAPK pathway and enhance growth. *Nature* **464**, 431-5 (2010).
36. Holderfield, M. et al. RAF inhibitors activate the MAPK pathway by relieving inhibitory autophosphorylation. *Cancer Cell* **23**, 594-602 (2013).

37. Mercer, K. et al. Expression of endogenous oncogenic V600EB-raf induces proliferation and developmental defects in mice and transformation of primary fibroblasts. *Cancer Res* **65**, 11493-500 (2005).
38. Harfe, B.D. et al. Evidence for an expansion-based temporal Shh gradient in specifying vertebrate digit identities. *Cell* **118**, 517-28 (2004).
39. Jaks, V. et al. Lgr5 marks cycling, yet long-lived, hair follicle stem cells. *Nat Genet* **40**, 1291-9 (2008).
40. Barker, N. et al. Identification of stem cells in small intestine and colon by marker gene Lgr5. *Nature* **449**, 1003-7 (2007).
41. Oshimori, N. & Fuchs, E. Paracrine TGF-beta signaling counterbalances BMP-mediated repression in hair follicle stem cell activation. *Cell Stem Cell* **10**, 63-75 (2012).
42. Nakao, A. et al. Identification of Smad7, a TGFbeta-inducible antagonist of TGF-beta signalling. *Nature* **389**, 631-5 (1997).
43. Jayaraman, S.S., Rayhan, D.J., Hazany, S. & Kolodney, M.S. Mutational landscape of basal cell carcinomas by whole-exome sequencing. *J Invest Dermatol* **134**, 213-20 (2014).
44. Hudson, A.M. et al. Discrepancies in cancer genomic sequencing highlight opportunities for driver mutation discovery. *Cancer Res* **74**, 6390-6 (2014).
45. Helleday, T., Eshtad, S. & Nik-Zainal, S. Mechanisms underlying mutational signatures in human cancers. *Nat Rev Genet* **15**, 585-98 (2014).
46. Wang, N.J. et al. Loss-of-function mutations in Notch receptors in cutaneous and lung squamous cell carcinoma. *Proc Natl Acad Sci U S A* **108**, 17761-6 (2011).
47. Goudie, D.R. et al. Multiple self-healing squamous epithelioma is caused by a disease-specific spectrum of mutations in TGFBR1. *Nat Genet* **43**, 365-9 (2011).
48. Glick, A.B. The Role of TGFbeta Signaling in Squamous Cell Cancer: Lessons from Mouse Models. *J Skin Cancer* **2012**, 249063 (2012).
49. Oshimori, N., Oristian, D. & Fuchs, E. TGF-beta promotes heterogeneity and drug resistance in squamous cell carcinoma. *Cell* **160**, 963-76 (2015).
50. White, R.A. et al. Epithelial stem cell mutations that promote squamous cell carcinoma metastasis. *J Clin Invest* **123**, 4390-404 (2013).
51. Connolly, E.C. & Akhurst, R.J. The complexities of TGF-beta action during mammary and squamous cell carcinogenesis. *Curr Pharm Biotechnol* **12**, 2138-49 (2011).
52. Oshimori, N. & Fuchs, E. The harmonies played by TGF-beta in stem cell biology. *Cell Stem Cell* **11**, 751-64 (2012).
53. White, A.C. et al. Stem cell quiescence acts as a tumour suppressor in squamous tumours. *Nat Cell Biol* **16**, 99-107 (2014).
54. Morris, J.C. et al. Phase I study of GC1008 (fresolimumab): a human anti-transforming growth factor-beta (TGFbeta) monoclonal antibody in patients with advanced malignant melanoma or renal cell carcinoma. *PLoS One* **9**, e90353 (2014).
55. Rheinwald, J.G. & Green, H. Serial cultivation of strains of human epidermal keratinocytes: the formation of keratinizing colonies from single cells. *Cell* **6**, 331-43 (1975).
56. Kluk, M.J. et al. Gauging NOTCH1 Activation in Cancer Using Immunohistochemistry. *PLoS One* **8**, e67306 (2013).
57. Li, H. et al. The Sequence Alignment/Map format and SAMtools. *Bioinformatics* **25**, 2078-9 (2009).
58. Forbes, S.A. et al. The Catalogue of Somatic Mutations in Cancer (COSMIC). *Curr Protoc Hum Genet* **Chapter 10**, Unit 10 11 (2008).

59. Okosun, J. et al. Integrated genomic analysis identifies recurrent mutations and evolution patterns driving the initiation and progression of follicular lymphoma. *Nat Genet* **46**, 176-81 (2014).
60. Saunders, C.T. et al. Strelka: accurate somatic small-variant calling from sequenced tumor-normal sample pairs. *Bioinformatics* **28**, 1811-7 (2012).
61. Lo Nigro, C. et al. Methylated tissue factor pathway inhibitor 2 (TFPI2) DNA in serum is a biomarker of metastatic melanoma. *The Journal of investigative dermatology* **133**, 1278-85 (2013).
62. Koboldt, D.C. et al. VarScan 2: somatic mutation and copy number alteration discovery in cancer by exome sequencing. *Genome Res* **22**, 568-76 (2012).
63. Van Loo, P. et al. Allele-specific copy number analysis of tumors. *Proc Natl Acad Sci U S A* **107**, 16910-5 (2010).
64. Okosun, J. et al. Recurrent mTORC1-activating RRAGC mutations in follicular lymphoma. *Nat Genet* **48**, 183-8 (2016).
65. Jackson, E.L. et al. Analysis of lung tumor initiation and progression using conditional expression of oncogenic K-ras. *Genes & development* **15**, 3243-8 (2001).
66. Luche, H., Weber, O., Nageswara Rao, T., Blum, C. & Fehling, H.J. Faithful activation of an extra-bright red fluorescent protein in "knock-in" Cre-reporter mice ideally suited for lineage tracing studies. *Eur J Immunol* **37**, 43-53 (2007).
67. Nowak, J.A. & Fuchs, E. Isolation and culture of epithelial stem cells. *Methods Mol Biol* **482**, 215-32 (2009).
68. Inman, G.J. et al. SB-431542 is a potent and specific inhibitor of transforming growth factor-beta superfamily type I activin receptor-like kinase (ALK) receptors ALK4, ALK5, and ALK7. *Mol Pharmacol* **62**, 65-74 (2002).

Acknowledgments

OS is supported by a Cancer Research UK core grant (A21139) and an ERC starting grant (311301). PC is supported by FP7 Health CP-IP - Large-scale integrating project grant (278568), DFV is supported by ERC Starting grant (311301). AMR is supported by Cancer Research UK centre grant (A12976). LCS was supported by WWCR grant 11-0788. GJI was supported by WWCR fellowship (03-0900). GJI, IML, CMP, CAH, KJP, AM, CP and APS were supported by a Cancer Research UK programme grant (A21358) and an ERC grant (250170).

Thanks to the research and scientific services at the CRUK Beatson Institute in general.

Author Contributions

OJS, GJI, PC, AMR, DV, JW and APS contributed to study design; PC, AMR, DFV, SL, DA contributed to the data acquisition ; PC, AMR, DFV, JW, AN, SL, RAR, DA, PJCV, AM, CP, JHSD, JL, SW, LCS, GPS, KJP, CMP, CAH, IRL, HC, NB, SK, CP, RM, CC, APS, OJS, GJI contributed to the data analysis and interpretation of the data; OJS, GJI, PC, AMR, APS, JW to drafting the manuscript.

Competing financial interests: the authors declare that they have no competing financial interest.

Figure Legends

Figure 1. **TGFβ receptors are frequently mutated in vemurafenib-induced skin lesions and sporadic cSCC tumors.** Mutation frequency, distribution and relationship with pathological features of skin lesions isolated from vemurafenib treated patients (n=39) (**a**), sporadic cSCC (n=91) (**b**), 21 cSCC cell lines (RDEB = recessive dystrophic epidermolysis bullosa) (**c**), (a-c, adapted from J Invest Dermatol. (2014) with permission from Elsevier (ref 6) and 7 sporadic cSCC tumors (T) and normal distant/perilesional skin samples (N) collected in Dundee (**d**). Mutation status for nine genes is indicated and the overall percentage mutation is shown on the left. Each column represents a single case. Colors correspond to specific mutations as shown. Details of clinical parameters are included in Supplementary Tables 1-3 and mutations are included in **Supplementary Data 1-5**.

Figure 2. Target gene mutation and copy number and clonality analysis in 30 cSCC primary tumors analysed by whole exome sequencing. (**a**) Mutation frequency, distribution and relationship with pathological features from 30 cSCC primary tumors. Mutation and copy number status (gain, loss and aUPD) for nine genes is indicated and the overall percentage alteration is shown on the left. Each column represents a single case. Colors correspond to specific mutations and copy number changes as shown. Split columns indicate where more than one mutation type is present in a single case. Details of clinical parameters and mutations are included in **Supplementary Table 4 and Supplementary Data 7**. (**b**) ABSOLUTE clonality analysis of potential driver genes of cSCC indicates that all nine genes are frequently clonal. (**c**) Cancer cell fraction clonality analysis indicates clonal and subclonal mutations in the indicated tumors.

Figure 3. Mutational frequencies and spectrum of driver mutations. Ranked driver gene mutations by (**a**) % VAF (p-values represent student's *t*-test (2-tailed) are shown above the figure, (**b**) % UV spectrum **(c)** predicted mutational consequence of Damaging/Non-damaging and (**d**) combined UV and damaging analysis (p-values are shown above the figure and represent Chi-squared *Fishers exact*-test). For all statistics; * defines statistical significance (*** p<0.001, ** p<0.01 and * P<0.05). Numbers of samples are contained in Supplementary Data 13. (**e**) Domain structures of TGFBR1 and TGFBR2 are shown. Exons are numbered and functional domains colour coded (see key). SNPs identified in TGFBR1 and TGFBR2 are labelled in AA sequence [using UniProtKB codes: P-36897-1, TGFBR1, HUMAN and P37173, P37173-2, TGFBR2_HUMAN] for sporadic cSCC (above) and Vemurafenib associated cSCC (below). Asterisked SNPs are those found in cSCC cell lines. Amino acid numbers for TGFBR2 refer to isoform 2.

Figure 4. Mutation of TGFβ receptors results in loss of function. (**a**) Indicated TGFBR1 plasmids were co-transfected into TGFBR1 null MEFs and assayed for SMAD7-Promoter Luciferase (SMAD7-Luc) reporter gene activity and receptor expression levels by western blot (lower panels) with and without TGFβ stimulation for 4 hours. β-ACTIN is used as a loading control. EV is empty vector control, WT is wild type. Data are mean +/- s.d., n=3. (**b**) Indicated TGFBR2 plasmids were co-transfected into TGFBR2 null T47D cells and assayed for SMAD7-Promoter Luciferase (SMAD7-Luc) reporter gene activity and receptor expression levels by western blot (lower panels) with and without TGFβ stimulation for 4 hours. β-ACTIN is used as a loading control. EV is empty vector control, WT is wild type. Data are mean +/- s.d., n=3. (**c**) PO_4-SMAD3 activity was assessed by IHC in wild type and mutant

tumors (n=8, ***= p=0.001, Mann-Whitney *U* test) Representative images are shown. Scale bar, 100 μM. (**d**) Effects of TGFβ stimulation on growth of NHK and cSCC cell lines. Data represent Cell Titre Glo™ measurement of cell proliferation over the indicated time course of cells treated with the indicated dose of TGFβ1. Normal human keratinocytes (NHK) and cell lines harbouring mutant TGFBR2 (SCCIC8, SCCIC12) are shown. Data represent the mean +/- s.d. n=6. (**e**) Restoration of wild type TGFBR2 restores growth inhibition. SCC1C8 and SCCIC12 cells were co-transfected with empty vector control (EV) or wild type TGFBR2 expression plasmids (TGFBR2) and a GFP expression plasmid. Proliferation of GFP^{+ve} cells was assessed using real-time Incucyte Zoom™ imaging over 6 days. Data represent the mean +/- s.d. n=6. *, ** and *** = p< 0.05, p<0.01 and p<0.001 respectively (Student's *t*-test).

Figure 5. Transit-amplifying SHH positive cells do not allow cSCC development. (**a**) PO_4-SMAD3 IHC in anagen human (left panel) and mouse (right panel) hair follicles reveals immunoreactivity in the hair matrix. CTL connective tissue layer, ORS outer root sheath, IRS inner root sheath, DP dermal papilla. Scale bar, 100 μm (**b**) Kaplan-Meier survival curve of *ShhCre^{ER} Braf^{V600E}* (n=13)*, ShhCre^{ER} Braf^{V600E} Tgfbr1$^{fl/+}$* (n=28) and *ShhCre^{ER} Braf^{V600E} Tgfbr1$^{fl/fl}$* (n=39) mice. (**c**) Kaplan-Meier survival curve of *ShhCre^{ER} Kras^{G12D}* (n=17) and *ShhCre^{ER} Kras^{G12D} Tgfbr1$^{fl/fl}$* (n=21) mice.

Figure 6. TGFβ signaling is active in $LGR5^{+ve}$ stem cells. (**a**) IHC analysis of PO_4-SMAD3 (left panels) and KERATIN 15 (right panels) in human normal skin. Insert shows strong PO_4-SMAD3 staining in the telogen hair follicle KERATIN 15^{+ve} bulge stem cells. Scale bar, 100 μm (**b**) IHC analysis of PO_4-SMAD3 (IFE inter-follicular epidermis, SG sebaceous gland, BG Bulge, DP dermal papilla) and (**c**) LGR5-GFP in murine skin in the telogen phase of the hair cycle.

Scale bar, 100 µm (**d**) Immunofluorescence (IF) analysis of LGR5-GFP and PO_4-SMAD3 in murine telogen skin. Nuclei are counterstained with DAPI. (**e**) Q-RTPCR analysis of *Tgfbr1*, *Tgfbr2*, *Tgfb1*, *Tgfb2*, *Tgfb3* and *Smad7* in LGR5^{+ve} (n=3 biological replicates) and LGR5^{-ve} cells (n=3 biological replicates) freshly isolated from back skin in the telogen phase. Data are shown as ratios to the internal *Gapdh* control with error bars representing s.e.m.. Statistical significance *p=0.04 (Mann-Whitney *U*-test, one-tailed test).

Figure 7. Deletion of *Tgfbr1* coupled with BRAF/KRAS activation leads to skin tumorigenesis. (**a**) Kaplan-Meier survival curve (left panel) of *Lgr5Cre^{ER} Tgfbr1$^{fl/fl}$* (n=12), *Lgr5Cre^{ER} Braf^{V600E}* (n=14), *Lgr5Cre^{ER} Braf^{V600E} Tgfbr1$^{fl/+}$* (n=23) and *Lgr5Cre^{ER} Braf^{V600E} Tgfbr1$^{fl/fl}$* (n=26) mice (p≤0.0001 by Log-Rank (Mantel-Cox)). Skin tumor free survival curve (right panel) of *Lgr5Cre^{ER} Braf^{V600E}* (n=5), *Lgr5Cre^{ER} Braf^{V600E} Tgfbr1$^{fl/+}$* (n=10) and *Lgr5Cre^{ER} Braf^{V600E} Tgfbr1$^{fl/fl}$* (n=19) mice. (**b**) Kaplan-Meier survival curve of *Lgr5Cre^{ER} Kras^{G12D}* (n=9) and *Lgr5Cre^{ER} Kras^{G12D} Tgfbr1$^{fl/fl}$* (n=14) mice (p<0.0001 by Log-Rank (Mantel-Cox)). (**c**) Macroscopic pictures of skin tumours from *Lgr5Cre^{ER} Braf^{V600E}*, *Lgr5Cre^{ER} Braf^{V600E} Tgfbr1$^{fl/+}$*, *Lgr5Cre^{ER} Braf^{V600E} Tgfbr1$^{fl/fl}$* and *Lgr5Cre^{ER} Kras^{G12D} Tgfbr1$^{fl/fl}$* mice. (**d**) Representative staining of KERATIN 1 (K1) and (**e**) KERATIN 5 (K5) on *Lgr5Cre^{ER} Braf^{V600E}*, *Lgr5Cre^{ER} Braf^{V600E} Tgfbr1$^{fl/+}$*, *Lgr5Cre^{ER} Braf^{V600E} Tgfbr1$^{fl/fl}$* and *Lgr5Cre^{ER} Kras^{G12D} Tgfbr1$^{fl/fl}$* mice. Scale bar, 100 µm.

Figure 8. Deletion of *Tgfbr1* coupled with *Tp53* mutation/deletion leads to skin tumorigenesis. (**a**) Kaplan-Meier survival curve of *Lgr5Cre^{ER} Tp53$^{R172H/fl}$* (n=31), *Lgr5Cre^{ER} Tp53$^{R172/+}$ Tgfbr1$^{fl/fl}$* (n=10) and *Lgr5Cre^{ER} Tp53$^{fl/+}$ Tgfbr1$^{fl/fl}$* (n=5) and *Lgr5Cre^{ER} Tp53$^{R172H/fl}$ Tgfbr1$^{fl/fl}$* (n=11) mice (p≤0.0001 by Log-Rank (Mantel-Cox)). (**b**) Tumor number of indicated

genotypes. (**c**) Macroscopic picture of a *Lgr5Cre*^{ER} *Tp53*$^{R172H/fl}$ *Tgfbr1*$^{fl/fl}$ mouse with a skin tumour. Representative staining of H&E, KERATIN 1 (K1) and KERATIN 5 (K5) is shown. Scale bar, 100 µm.

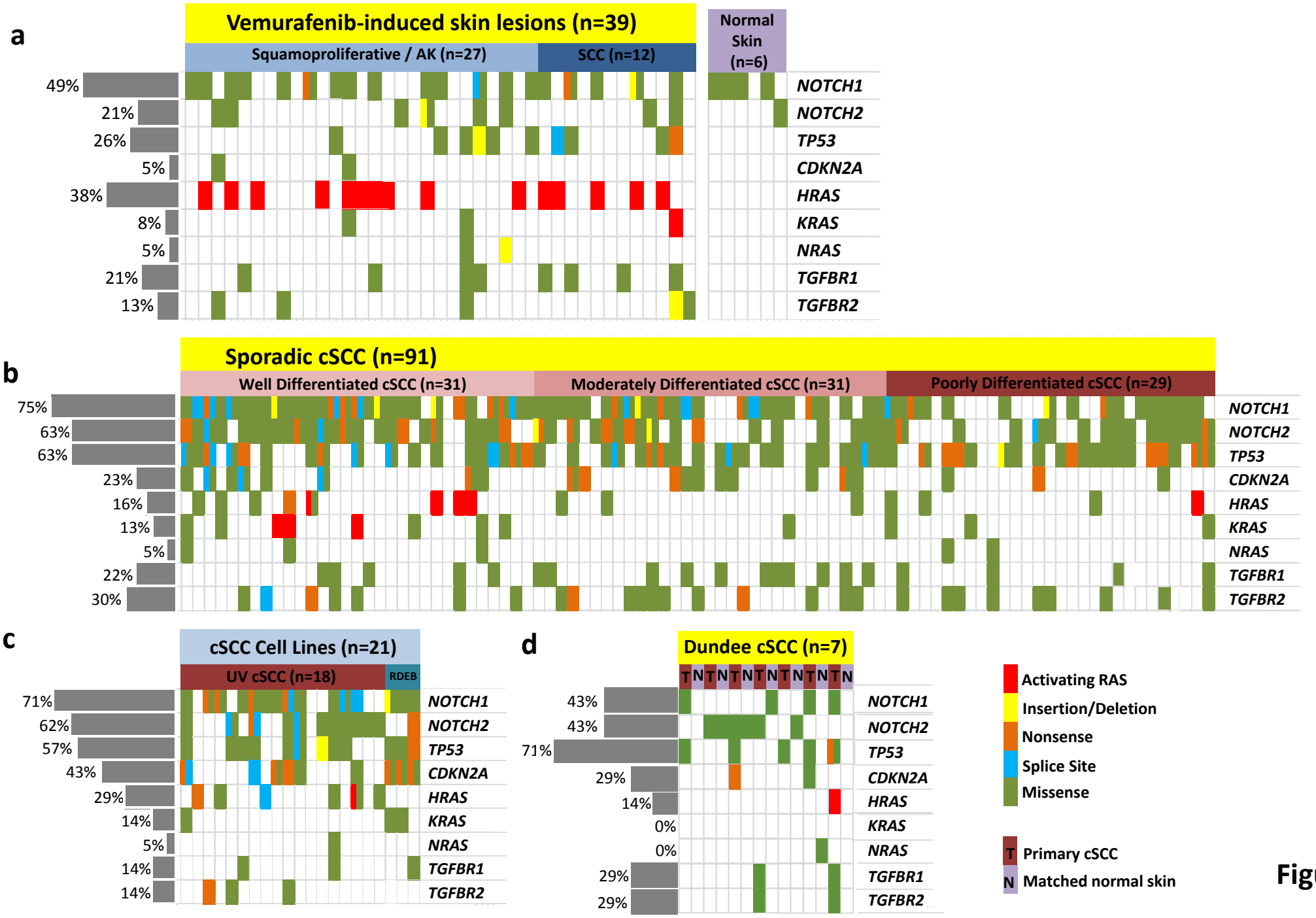
a
Vemurafenib-induced skin lesions (n=39)
Squamoproliferative / AK (n=27)
SCC (n=12)
Normal Skin (n=6)
49%
21%
26%
5%
38%
8%
5%
21%
13%
NOTCH1
NOTCH2
TP53
CDKN2A
HRAS
KRAS
NRAS
TGFBR1
TGFBR2
b
Sporadic cSCC (n=91)
Well Differentiated cSCC (n=31)
Moderately Differentiated cSCC (n=31)
Poorly Differentiated cSCC (n=29)
75%
63%
63%
23%
16%
13%
5%
22%
30%
NOTCH1
NOTCH2
TP53
CDKN2A
HRAS
KRAS
NRAS
TGFBR1
TGFBR2
c
cSCC Cell Lines (n=21)
UV cSCC (n=18)
RDEB
71%
62%
57%
43%
29%
14%
5%
14%
14%
NOTCH1
NOTCH2
TP53
CDKN2A
HRAS
KRAS
NRAS
TGFBR1
TGFBR2
d
Dundee cSCC (n=7)
T N T N T N T N T N T N T N
43%
43%
71%
29%
14%
0%
0%
29%
29%
NOTCH1
NOTCH2
TP53
CDKN2A
HRAS
KRAS
NRAS
TGFBR1
TGFBR2
Activating RAS
Insertion/Deletion
Nonsense
Splice Site
Missense
T Primary cSCC
N Matched normal skin

Figure 1

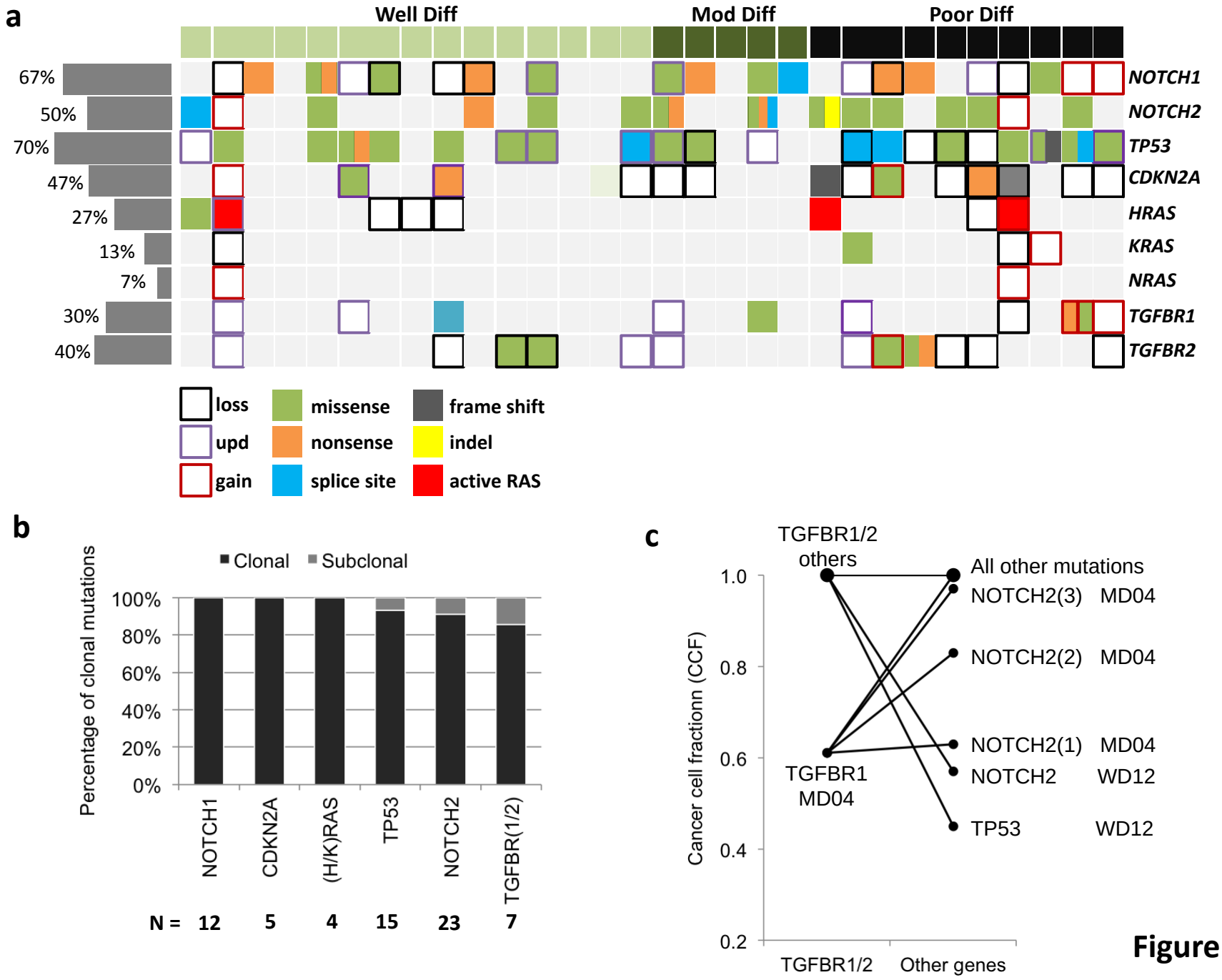
a
Well Diff
Mod Diff
Poor Diff
67%
50%
70%
47%
27%
13%
7%
30%
40%
NOTCH1
NOTCH2
TP53
CDKN2A
HRAS
KRAS
NRAS
TGFBR1
TGFBR2
loss
upd
gain
missense
nonsense
splice site
frame shift
indel
active RAS
b
Clonal
Subclonal
Percentage of clonal mutations
100%
80%
60%
40%
20%
0%
NOTCH1
CDKN2A
(H/K)RAS
TP53
NOTCH2
TGFBR(1/2)
N = 12 5 4 15 23 7
c
TGFBR1/2
others
TGFBR1
MD04
All other mutations
NOTCH2(3) MD04
NOTCH2(2) MD04
NOTCH2(1) MD04
NOTCH2 WD12
TP53 WD12
Cancer cell fractionn (CCF)
1.0
0.8
0.6
0.4
0.2
TGFBR1/2
Other genes

Figure 2

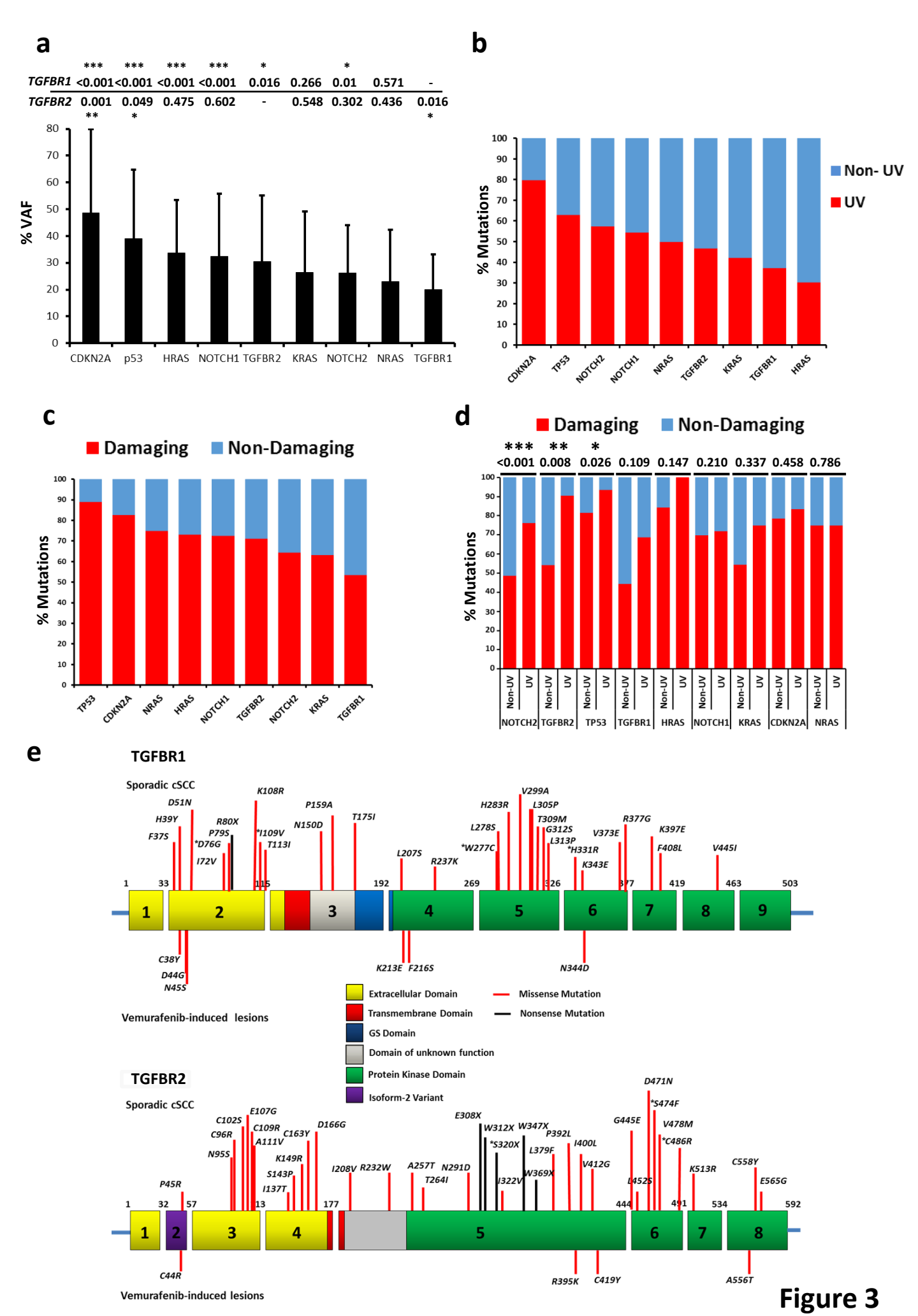
a
TGFBR1 <0.001 <0.001 <0.001 <0.001 0.016 0.266 0.01 0.571 -
TGFBR2 0.001 0.049 0.475 0.602 - 0.548 0.302 0.436 0.016
% VAF
CDKN2A p53 HRAS NOTCH1 TGFBR2 KRAS NOTCH2 NRAS TGFBR1
b
% Mutations
Non- UV
UV
CDKN2A TP53 NOTCH2 NOTCH1 NRAS TGFBR2 KRAS TGFBR1 HRAS
c
Damaging
Non-Damaging
% Mutations
TP53 CDKN2A NRAS HRAS NOTCH1 TGFBR2 NOTCH2 KRAS TGFBR1
d
Damaging
Non-Damaging
<0.001 0.008 0.026 0.109 0.147 0.210 0.337 0.458 0.786
% Mutations
Non-UV UV
NOTCH2 TGFBR2 TP53 TGFBR1 HRAS NOTCH1 KRAS CDKN2A NRAS
e
TGFBR1
Sporadic cSCC
Vemurafenib-induced lesions
Extracellular Domain
Transmembrane Domain
GS Domain
Domain of unknown function
Protein Kinase Domain
Isoform-2 Variant
Missense Mutation
Nonsense Mutation
TGFBR2
Sporadic cSCC
Vemurafenib-induced lesions

Figure 3

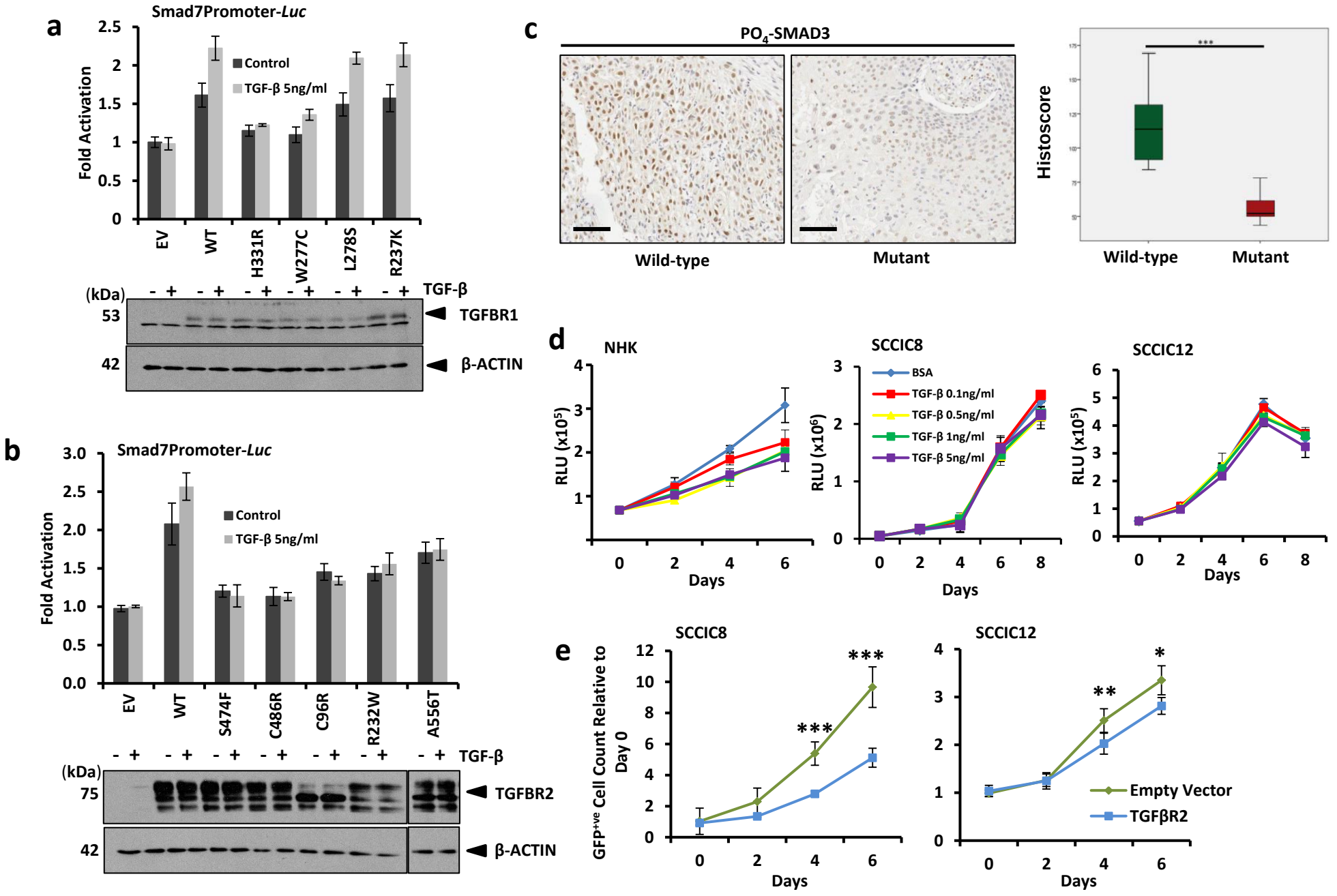
a
Smad7Promoter-Luc
Fold Activation
Control
TGF-β 5ng/ml
EV
WT
H331R
W277C
L278S
R237K
(kDa)
TGF-β
53
TGFBR1
42
β-ACTIN
b
Smad7Promoter-Luc
Fold Activation
Control
TGF-β 5ng/ml
EV
WT
S474F
C486R
C96R
R232W
A556T
(kDa)
TGF-β
75
TGFBR2
42
β-ACTIN
c
PO4-SMAD3
Wild-type
Mutant
Histoscore
***
Wild-type
Mutant
d
NHK
SCCIC8
SCCIC12
RLU (x10^5)
RLU (x10^6)
Days
BSA
TGF-β 0.1ng/ml
TGF-β 0.5ng/ml
TGF-β 1ng/ml
TGF-β 5ng/ml
e
SCCIC8
SCCIC12
GFP+ve Cell Count Relative to Day 0
Days
Empty Vector
TGFβR2

Figure 4

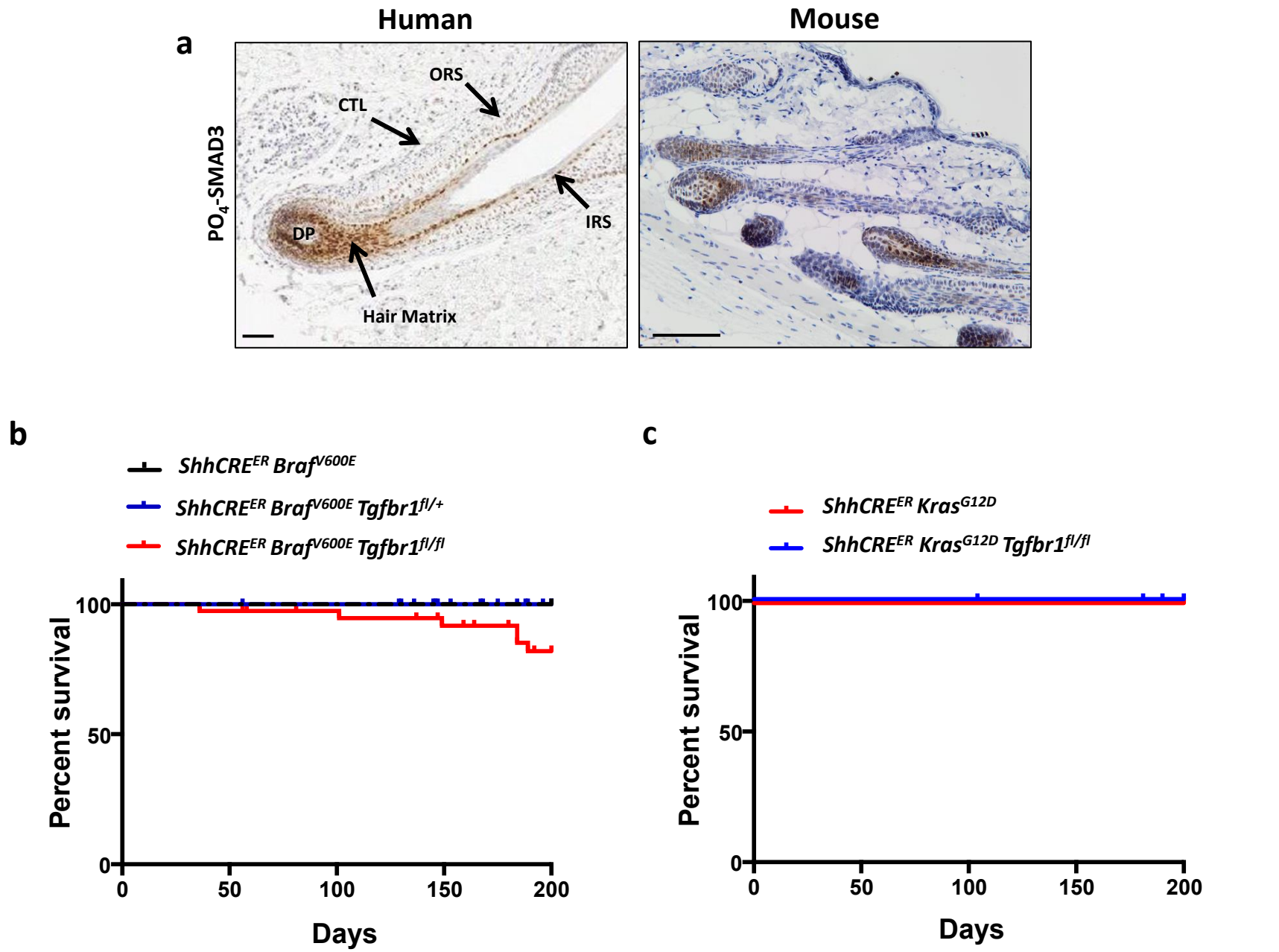
a
Human
Mouse
PO4-SMAD3
ORS
CTL
IRS
DP
Hair Matrix
b
ShhCREER BrafV600E
ShhCREER BrafV600E Tgfbr1fl/+
ShhCREER BrafV600E Tgfbr1fl/fl
Percent survival
100
50
0
0
50
100
150
200
Days
c
ShhCREER KrasG12D
ShhCREER KrasG12D Tgfbr1fl/fl
Percent survival
100
50
0
0
50
100
150
200
Days

Figure 5

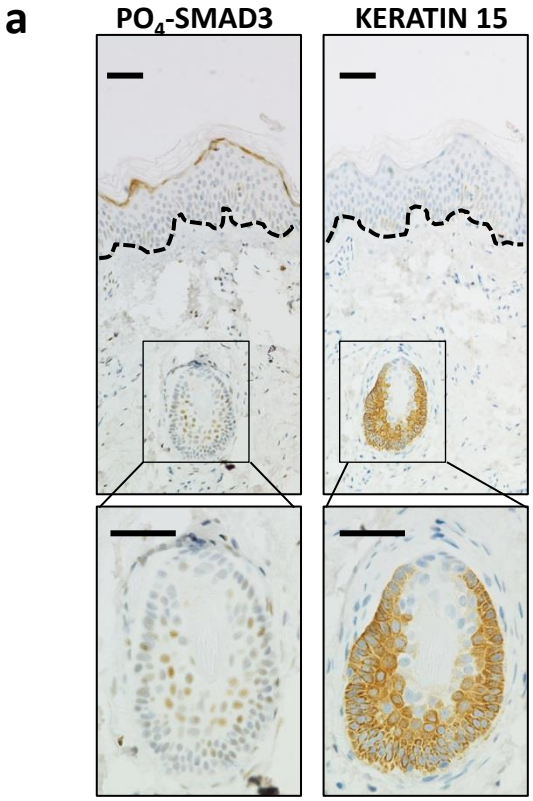
a
PO4-SMAD3
KERATIN 15

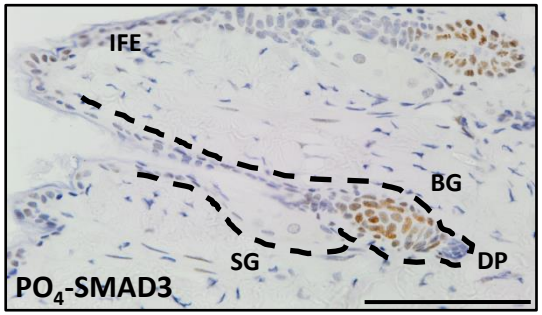
b
IFE
BG
SG
DP
PO4-SMAD3

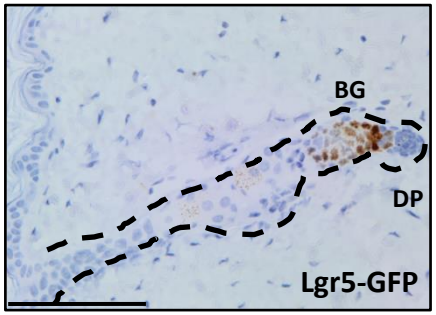
c
BG
DP
Lgr5-GFP

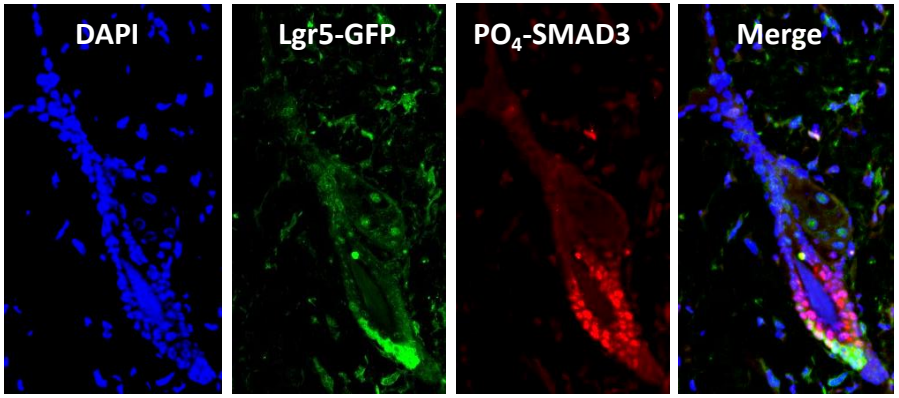
d
DAPI
Lgr5-GFP
PO4-SMAD3
Merge

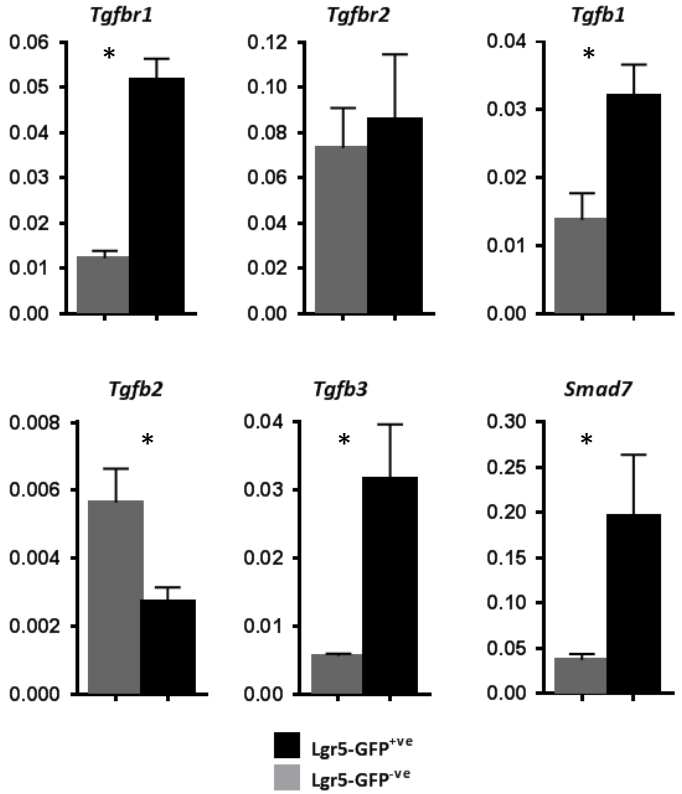
e
Tgfbr1
Tgfbr2
Tgfb1
Tgfb2
Tgfb3
Smad7
Lgr5-GFP+ve
Lgr5-GFP-ve

Figure 6

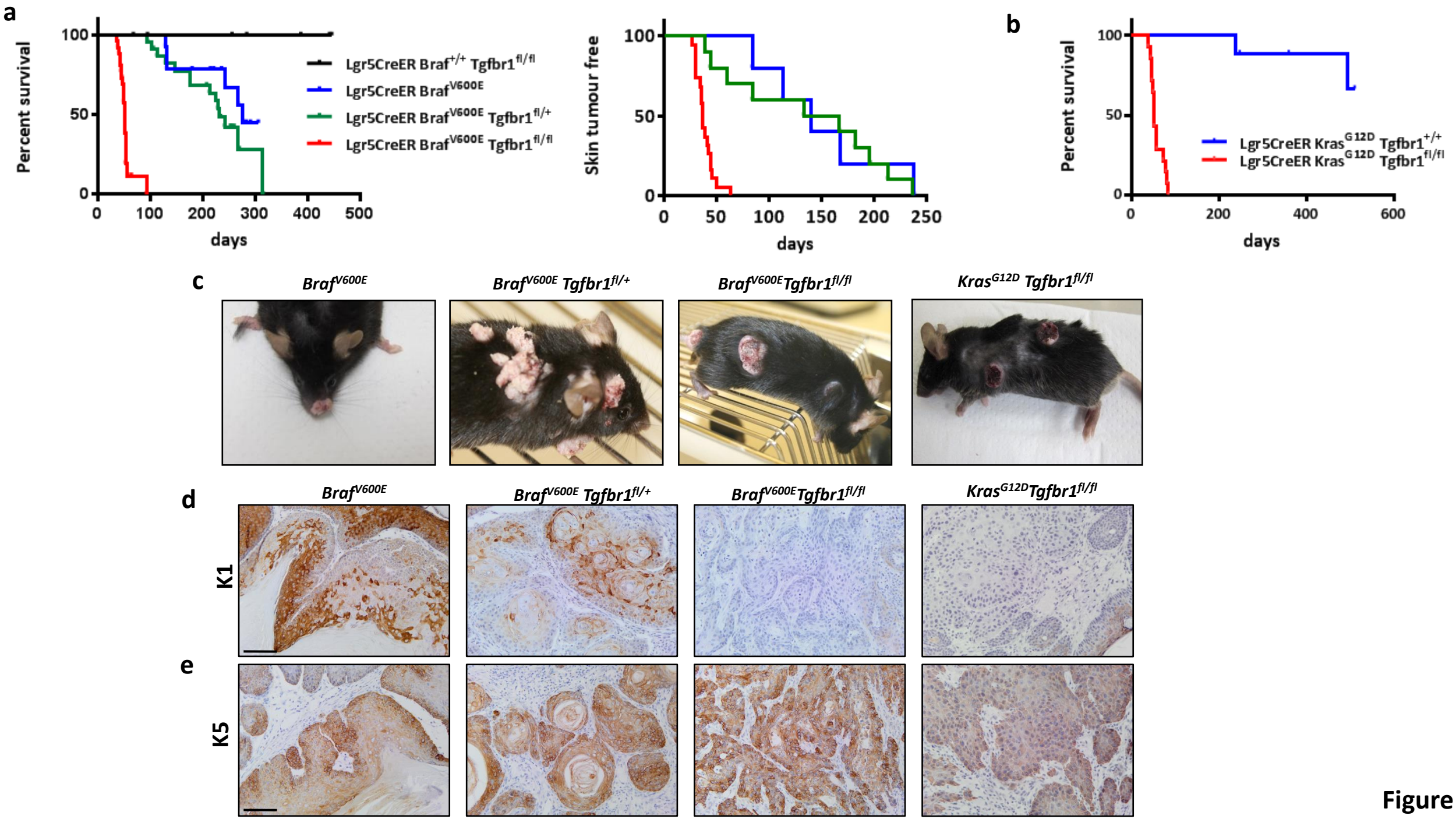
a
Percent survival
100
50
0
0
100
200
300
400
500
days
Lgr5CreER Braf+/+ Tgfbr1fl/fl
Lgr5CreER BrafV600E
Lgr5CreER BrafV600E Tgfbr1fl/+
Lgr5CreER BrafV600E Tgfbr1fl/fl
Skin tumour free
100
50
0
0
50
100
150
200
250
days
b
Percent survival
100
50
0
0
200
400
600
days
Lgr5CreER KrasG12D Tgfbr1+/+
Lgr5CreER KrasG12D Tgfbr1fl/fl
c
BrafV600E
BrafV600E Tgfbr1fl/+
BrafV600E Tgfbr1fl/fl
KrasG12D Tgfbr1fl/fl
d
BrafV600E
BrafV600E Tgfbr1fl/+
BrafV600E Tgfbr1fl/fl
KrasG12D Tgfbr1fl/fl
K1
e
K5

Figure 7

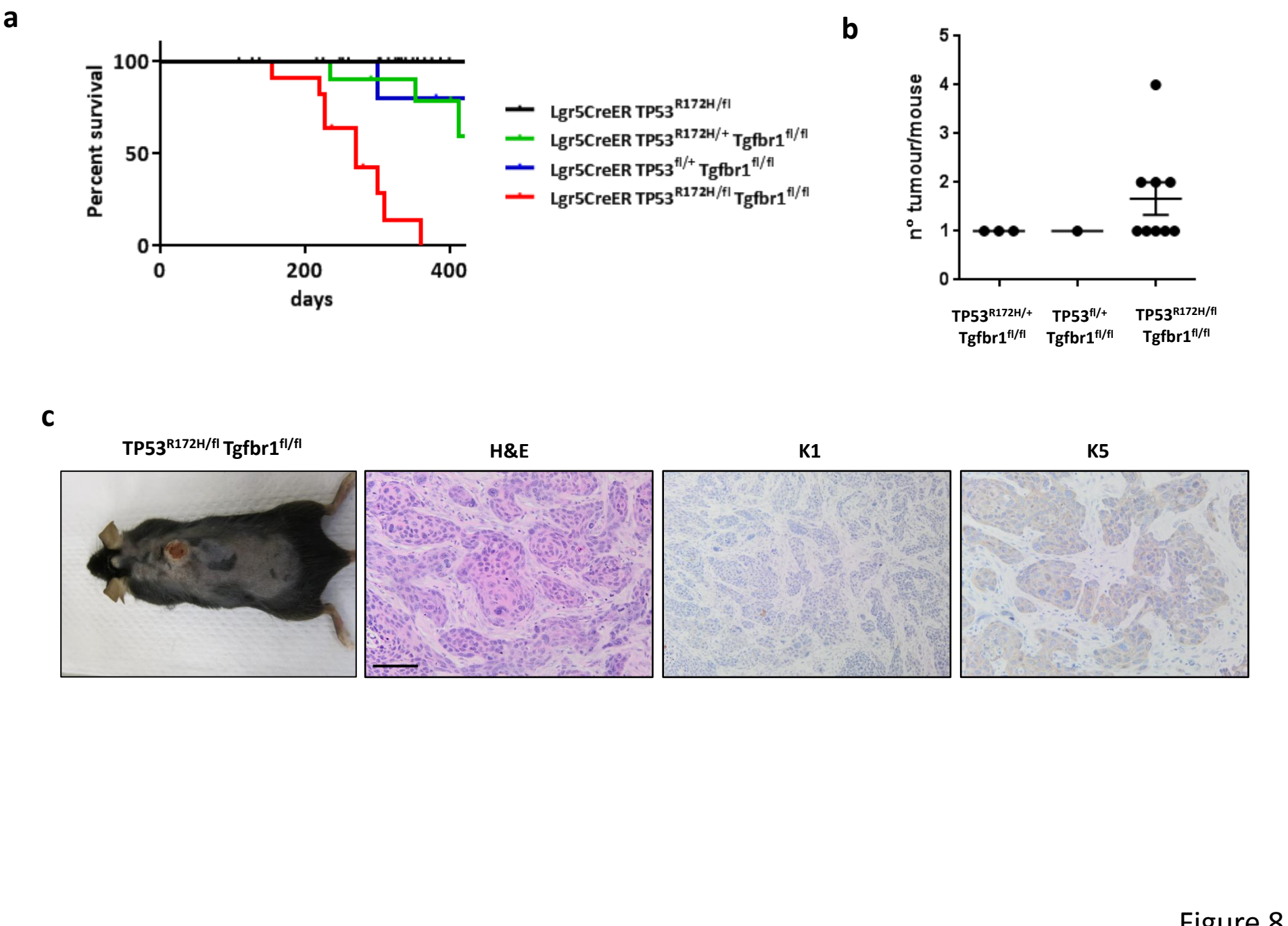
a
Percent survival
100
50
0
0
200
400
days
Lgr5CreER TP53R172H/fl
Lgr5CreER TP53R172H/+ Tgfbr1fl/fl
Lgr5CreER TP53fl/+ Tgfbr1fl/fl
Lgr5CreER TP53R172H/fl Tgfbr1fl/fl
b
n° tumour/mouse
5
4
3
2
1
0
TP53R172H/+ Tgfbr1fl/fl
TP53fl/+ Tgfbr1fl/fl
TP53R172H/fl Tgfbr1fl/fl
c
TP53R172H/fl Tgfbr1fl/fl
H&E
K1
K5

Figure 8